Wireless Communications and Mobile Computing

Communications and Networking for Connected Vehicles 2022

Lead Guest Editor: Li Zhu
Guest Editors: Richard Yu, Victor Leung, and Meng Li

Communications and Networking for Connected Vehicles 2022

Wireless Communications and Mobile Computing

Communications and Networking for Connected Vehicles 2022

Lead Guest Editor: Li Zhu
Guest Editors: Richard Yu, Victor Leung, and Meng Li

Chief Editor

Associate Editors

Academic Editors

Contents

Hindawi
Wireless Communications and Mobile Computing
Volume 2023, Article ID 4352786, 8 pages
https://doi.org/10.1155/2023/4352786

Research Article

Multiband Cooperative Spectrum Sensing Meets Vehicular Network: Relying on CNN-LSTM Approach

Lingyun Lu,[1] Xiang Li,[2] Guizhu Wang,[3] and Wei Ni[4]

[1]*School of Software Engineering, Beijing Jiaotong University, Beijing 100091, China*
[2]*School of Computer and Information Technology, Beijing Jiaotong University, Beijing 100091, China*
[3]*Rizhao Big Data Development Bureau, Rizhao 276826, China*
[4]*The Commonwealth Scientific and Industrial Research Organisation, Sydney, Australia*

Correspondence should be addressed to Xiang Li; 19112017@bjtu.edu.cn

Received 29 November 2022; Revised 6 March 2023; Accepted 2 June 2023; Published 16 June 2023

Academic Editor: Meng Li

A vehicular network is expected to empower all aspects of the intelligent transportation system (ITS) and aim at improving road safety and traffic efficiency. In view of the fact that spectrum scarcity becomes more severe owing to the increasing number of connected vehicles, implying spectrum sensing technology in vehicular network, i.e., cognitive vehicular network, has emerged as a promising solution to provide opportunistic usage of licensed spectrum. However, some unique features of vehicular networks, such as high movement and dynamic topology, take on high challenges for spectrum sensing. Recently, machine learning-based approaches, especially deep learning, for spectrum sensing have attracted sufficient interest. In this work, we investigate a learning-based cooperative spectrum sensing (CSS) approach for multiband spectrum sensing in the cognitive vehicular network. Specifically, we integrate two powerful deep learning models, i.e., the convolutional neural network (CNN) to exploit the features from sensing data, and the long-short-term memory (LSTM) network is then utilized to extract temporal correlations given input as the generated features by the CNN structure. Instead of the predefined decision threshold typically set in conventional approaches, our proposed approach could eliminate the impact of impertinent threshold value setting. Extensive simulations have been conducted to evaluate the effectiveness of the proposed method in achieving satisfactory spectrum sensing performance, particularly in terms of higher detection accuracy, robustness in low signal-to-noise ratio (SNR) environments, and a significant reduction in spectrum sensing time compared to other methods.

1. Introduction

The unprecedented development of intelligent transportation system (ITS) and various vehicular applications magnifies the scarcity of available spectrum resources. Meanwhile, in light of the fact that the licensed spectrum is usually not fully utilized, cognitive radio (CR) has been recognized as a promising solution to improve spectrum utilization. As the core technique of CR, spectrum sensing (SS) plays a key role in identifying the spectrum occupancy state associated with licensed users (i.e., primary users and PUs). The unlicensed users, called secondary users (SUs), are allowed to opportunistically access the spectrum that is not occupied by its incumbent PU. During the past decades, a variety of research works on effective spectrum sensing have been fully studied in conventional wireless network. Nevertheless, it is still in the development stage to implement spectrum sensing in vehicular network due to a series of challenges brought on by the high-speed movement of vehicles, such as the fluctuation of wireless communication channels, the dynamics of the network topology, and the diverse environments where the vehicular network is located [1].

Conventional spectrum sensing schemes typically rely on well-designed test statistics based on received sensing signals and then compare them with a predefined threshold to check the spectrum availability. According to the requirement for a priori information about PU's signal (such as modulation type and grade, pulse shape, and frame format) and noise (e.g., channel model and power), those spectrum sensing schemes can be classified into three categories:

nonblind, semiblind, and completely blind. The nonblind spectrum sensing schemes require both accurate statistical models of the PU's signal and noise. For example, derived from the log-likelihood ratio (LLR) detection, the estimator-correlator (E-C) detection has been proved to achieve the theoretical optimum [2] and provide perfect knowledge of both PU signals and noises. Accordingly, Gardner designed cyclostationary detection by exploiting the cyclostationarity attributes of received signals, which can differentiate noise from primary users' signals [3]. Similarly, matched filtering (MF) detection was proposed in [4] if certain PU signal information is known, but it requires perfect timing and synchronization which increases the calculation complexity. Among the semiblind schemes, energy detection (ED) is the most common way [5] which only needs the knowledge of noise power and thus has low implementation complexity. However, the performance of energy detection practically faces challenges due to the existence of noise uncertainty, and it fails to work when the signal-to-noise ratio (SNR) falls below some threshold, which is commonly known as the SNR-wall problem. To get rid of any a priori knowledge on PU signal or noise power, eigenvalue-based detection [6] and covariance matrix-based detection [7] are two preferred approaches with respect to the totally blind schemes. Although they reveal robustness against low SNR condition and noise uncertainty, extra computational cost is needed for computing the statistical covariance matrix and substantial eigenvalues. In conclusion, these works are mainly based on test statistic design with empirically statistical modeling, which might not perform favorably in a real-time-varying vehicular network, thus resulting in significant performance degradation.

In contrast to conventional model-driven methods, by exploiting the test statistics of received sensing signals, motivated by recent trends in machine learning (ML) applied to wireless communication which has proved great success, comprehensive learning-based applications for spectrum sensing have been advocated. The spectrum sensing process is equivalent to a binary classification problem in the context of ML. There are various studies related to ML models for spectrum sensing, which include but are not limited to the hidden Markov model (HMM), decision tree (DT), linear autoregressive model, support vector machine (SVM), and Gaussian mixture model (GMM). Specifically, deep learning (DL) presents an outstanding performance in many areas because of its powerful ability to extract complex features in a data-driven way. For example, to benefit from the powerful capability of convolutional neural network (CNN) in extracting features from matrix-shaped data, Liu et al. [8] dealed with the sample covariance matrix as the CNN input and proposed a covariance matrix-aware CNN (CM-CNN) method which significantly outperforms other spectrum sensing methods. Chen et al. [9] utilized the short-time Fourier transform (STFT) to obtain rich information by time-frequency analyses, and then a STFT-CNN spectrum sensing model was designed to extract the features of the time-frequency matrix and further improve the sensing accuracy under low SNR. Besides, to address the problem of labeled data shortage as vehicular network changes over time, Xie et al. [10] developed an unsupervised deep learning-based spectrum sensing method (UDSS), which established the variational autoencoder with the Gaussian mixture model that achieves close performance compared with the supervised learning-based benchmarks. Several works with a generative adversarial network (GAN) have been proposed to generate synthetic data for training when the number of training samples is insufficient and the spectrum sensing model can be retrained in a new environment, thus enhancing its adaptability [11, 12].

In practical wireless communication, the quality of PUs' signal detected at SUs is easily degraded; even SUs cannot receive PUs' signal which is known as the hidden node problem. Besides, the sensing reliability of individual SUs is susceptible to errors, leading to incorrect prediction of the occupancy state of the licensed spectrum. To overcome these issues, cooperative spectrum sensing (CSS) is viewed as a better solution, where all SUs exchange their sensing information with a fusion center (FC) for global decision-making. The FC might be part of the network infrastructure such as the wireless access point or one of the SUs. It combines the sensing information from all participating SUs, follows some fusion rules, analyzes the spectrum availability, and then feedbacks the prediction result of the spectrum occupancy state.

Despite the aforementioned studies, especially the usage of DL, which have shown extreme success in solving spectrum sensing problem, there are still many challenges that need to be solved urgently. One weakness of most spectrum sensing approaches is that they seldom consider the temporal correlation of received signals across multiple sensing periods. It has been reflected that when a PU turns from the silent state to the transmission state, it will probably stay in the transmission state for multiple sensing periods and vice versa [13, 14], thus the PU's pattern should be fully harnessed to improve the spectrum sensing performance. In addition, it is of vital importance to perform sensing over a wide frequency range, i.e., multiband spectrum sensing, whereas existing studies usually perform spectrum sensing over a single band. Intuitively, this problem can be addressed by converting it into a series of single-band spectrum sensing. However, implementing spectrum sensing in each subband independently may ignore the correlation between subbands.

In this paper, we consider multiband spectrum sensing utilizing deep learning models in a cooperative way. Specifically, considering that the covariance matrix of received signals has been inherent as the scope of interest input features in relative researches, we first propose a covariance matrix-aware CNN model, and then a LSTM shows a powerful capability to capture the temporal features from time series data. It is worth highlighting that the proposed detection does not require any additional information about the primary signal or noise density when deployed online. Through extensive simulation and comparison, the advantages of the proposed detection method are verified compared with traditional spectrum sensing methods. In addition, the effects of different false alarm probabilities, different sampling lengths, and different modulation types on the detection performance of the proposed model are also explored.

The remainder of this paper is organized as follows. Section 2 presents the system model. In Section 3, our proposed multiband cooperative spectrum sensing approach is described in detail. Extensive simulations are discussed in Section 4, followed by conclusions in Section 5.

2. System Model

As shown in Figure 1, we consider a multiband cognitive vehicular network consisting of M, PUs, and K cognitive vehicle users (CVU). The system spectrum is divided equally into Q nonoverlapping subbands. The set of PUs, CVUs, and available subbands is collected as $\mathcal{M}$, $\mathcal{K}$, and $\mathcal{Q}$, respectively. For convenience, we suppose each PU randomly selects a fixed number of Q_m consecutive subbands that can meet its communication requirement. Furthermore, the power leakage effect is considered, which means the occupied subbands with PU's signal may influence the adjacent idle subband [15], and the proportion of power leakage is set to η.

According to subband occupancy, an arbitrary subband q can be categorized into three cases: occupied by PU ($q \in \mathcal{Q}_o$), fully vacant ($q \in \mathcal{Q}_v$), and vacant but influenced by power leakage ($q \in \mathcal{Q}_{vp}$). In this paper, we consider the subband-occupied case as $\mathcal{H}_1$ hypothesis, and the other two cases are viewed as $\mathcal{H}_0$ hypothesis. An example of the possible spectrum occupancy state of two PUs is shown in Figure 2.

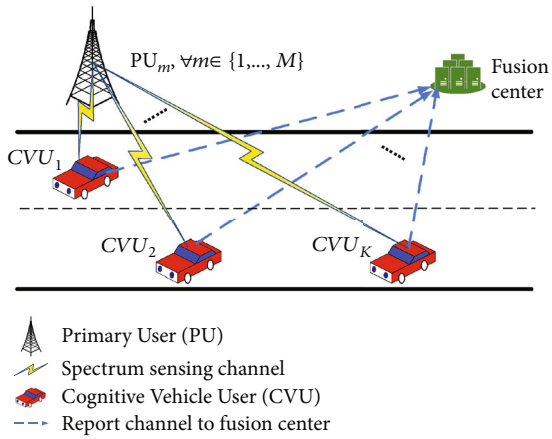

Figure 1: The cooperative spectrum sensing system for the cognitive vehicular network.

$$y_{k,n}(q) = \begin{cases} \sum_{m=1}^{M} \alpha_q^m \sqrt{P_{\mathrm{PU}}} h_{m,k}(q) s_{m,n} + w_n(q), & \text{case1} : q \in \mathcal{Q}_o, \\ \sqrt{\eta} \sum_{m=1}^{M} \alpha_{q_-}^m \sqrt{P_{\mathrm{PU}}} h_{m,k}(q_-) s_{m,n} + \sqrt{\eta} \sum_{m=1}^{M} \alpha_{q_+}^m \sqrt{P_{\mathrm{PU}}} h_{m,k}(q_+) s_{m,n} + w_n(q), & \text{case2} : q \in \mathcal{Q}_{vp} \\ w_n(q), & \text{case3} : q \in \mathcal{Q}_v. \end{cases} \quad (1)$$

During a spectrum sensing period, each CVU aims to perform spectrum sensing to decide vacant subbands for access through capturing N signal sampling on each subband. Therefore, the nth received a signal sample of the k th CVU on the qth subband can be represented as equation (1). Here, $w_n(q)$ is the additive noise on the subband q following the zero mean circularly symmetric complex Gaussian (CSCG) distribution with variance σ_ω^2. The binary indicator $\alpha_q^m \in \{0, 1\}$ means that the mth PU is inactive or active on the subband q, and it is limited that $\sum_{m=1}^{M} \alpha_q^m \leq 1$ indicating only one PU can access to individual subband in each sensing period to avoid mutual interference. The PUs' transmit power is fixed as $\sqrt{P_{\mathrm{PU}}}$, and $s_{m,n}$ is the transmit symbol of the mth PU at sampling time n. The variables q_- and q_+ denote two adjacent subbands of subband q, respectively. $h_{m,k}(q)$ denotes the channel gain from the mth PU to the kth CVU on a subband q modeled as

$$h_{m,k}(q) = \sqrt{\mathrm{PL}\left(\left\| c_m^{PU} - c_k^{CVU} \right\|_2\right)} \cdot \nu_{m,k}. \quad (2)$$

Here c_m^{PU} and c_k^{CVU} are the two-dimensional coordinates of PUs and CVUs, respectively. The operation $\|\cdot\|_2$ is to evaluate the Euclidean distance, and $\mathrm{PL}(d) = d^{-\beta}$ is the power loss in the propagation with regard to distance d and path-loss exponent β. $\nu_{m,k}$ represents the fading coefficient, and in this paper, it is assumed that the transmitted signal experiences a quasi-static channel. Therefore, the received sampling signal matrix of CVU k can be represented as $\mathbf{Y}_k = [\mathbf{y}_k(1) \cdots \mathbf{y}_k(q) \cdots \mathbf{y}_k(Q)]^T$, i.e.,

$$\mathbf{Y}_k = \begin{cases} y_{k,1}(1) & \cdots & y_{k,n}(1) & \cdots & y_{k,N}(1), \\ \vdots & \ddots & \vdots & \ddots & \vdots \\ y_{k,1}(q) & \cdots & y_{k,n}(q) & \cdots & y_{k,N}(q), \\ \vdots & \ddots & \vdots & \ddots & \vdots \\ y_{k,1}(Q) & \cdots & y_{k,n}(Q) & \cdots & y_{k,N}(Q). \end{cases} \quad (3)$$

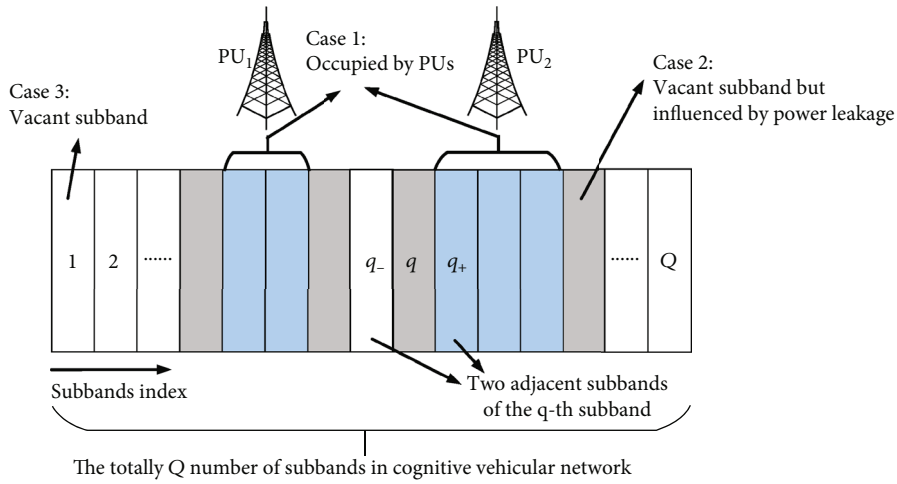

Figure 2: The illustration of the subband occupancy state of two PU systems.

3. The Proposed Multiband Cooperative Spectrum Sensing Approach Based on CNN-LSTM

The purpose of the spectrum sensing problem in the context of deep learning is equivalent to constructing a classifier, which can correctly map the collected K received signal vectors $\mathbf{Y}_k, \forall k \in \mathcal{K}$ to the subband occupancy state. In this section, we next illustrate the details of the proposed multiband cooperative spectrum sensing algorithm.

3.1. Data Preprocessing. Instead of utilizing the originally received sampling signal matrix for following spectrum sensing decision, we adopt sample covariance matrix transform, i.e., calculating the covariance matrix of each sample $\mathbf{y}_k(q), \forall q \in \mathcal{Q}$ on all subbands denoted as $\mathbf{R}_k(q)$.

$$\mathbf{R}_k(q) = \frac{1}{N}\mathbf{y}_k(q)\mathbf{y}_k^H(q). \tag{4}$$

Then, we concatenate the multiband covariance matrices as the collected feature matrix locally of the kth CVU, i.e.,

$$\mathbf{R}_k = \begin{bmatrix} \mathbf{R}_k(1) \\ \vdots \\ \mathbf{R}_k(q) \\ \vdots \\ \mathbf{R}_k(Q) \end{bmatrix}. \tag{5}$$

At each sensing period, the fusion center can collect all K local feature matrices $\{\mathbf{R}_k, \forall k \in \mathcal{K}\}$ and put them together as a feature matrix globally $\mathbf{X} = [\mathbf{R}_1 \cdots \mathbf{R}_k \cdots \mathbf{R}_K]$, which is viewed as the input of the learning module to perform multiband cooperative spectrum sensing.

$$\mathbf{X} = \begin{pmatrix} \mathbf{R}_1(1) & \cdots \mathbf{R}_k(1) & \cdots & \mathbf{R}_K(1) \\ \mathbf{R}_1(2) & \cdots \mathbf{R}_k(2) & \cdots & \mathbf{R}_K(2) \\ \vdots & \vdots & \vdots & \\ \mathbf{R}_1(Q) & \cdots \mathbf{R}_k(Q) & \cdots & \mathbf{R}_K(Q) \end{pmatrix}. \tag{6}$$

It is required to collect enough labeled training data firstly for execution following the deep learning approach. We first collect sensing data over T consecutive sensing periods, where each data consists of the global feature matrix and corresponding subband occupancy, i.e., $(\mathbf{X}^{(1)}, \mathbf{a}^{(1)}), \cdots, (\mathbf{X}^{(t)}, \mathbf{a}^{(t)}), \cdots, (\mathbf{X}^{(T)}, \mathbf{a}^{(T)})$. The subbands occupancy $\mathbf{a}^{(t)}$ is a vector with a length of Q, in which each element is 1 or 0 indicating the corresponding subband is or not be occupied. Furthermore, we rearrange those T number of consecutive sensing data in order to excavate the inherent pattern of PUs. Specifically, a sequence of λ length sensing data is combined, and we obtain the required training dataset $\mathbf{D} = (\mathbf{d}_1, \mathbf{b}_1), \cdots, (\mathbf{d}_u, \mathbf{b}_u), \cdots, (\mathbf{d}_U, \mathbf{b}_U)$, where $d_u = [\mathbf{X}^{(u)}, \mathbf{X}^{(u+1)}, \cdots, \mathbf{X}^{(u+\lambda-1)}]$ and $\mathbf{b}_u = \mathbf{a}^{(u+\lambda-1)}$. It means that the built classifier can predict current subband occupancy via both the current sensing feature vector and previous $\lambda - 1$ sensing feature vectors. The training dataset $\mathbf{D}$ for the following network training is built, which has $U = T - \lambda + 1$ number of training samples. The procedure of data preprocessing above is illustrated in Figure 3.

3.2. Network Structure and Learning Process. The network structure of the proposed learning approach is shown in Figure 4, which is inspired by [16]. The training sample d_u is in complex value and thus can be witnessed as a series of two-layer images with a length of λ. We first sequentially input the training sample into the CNN module which consists of two convolutional layers. Two parallel structures containing multiple convolution layers and max-pooling layers intake and process the observation of present and historical sensing periods. After the convolution-pooling structure, the outputs of the two parallel structures are flattened

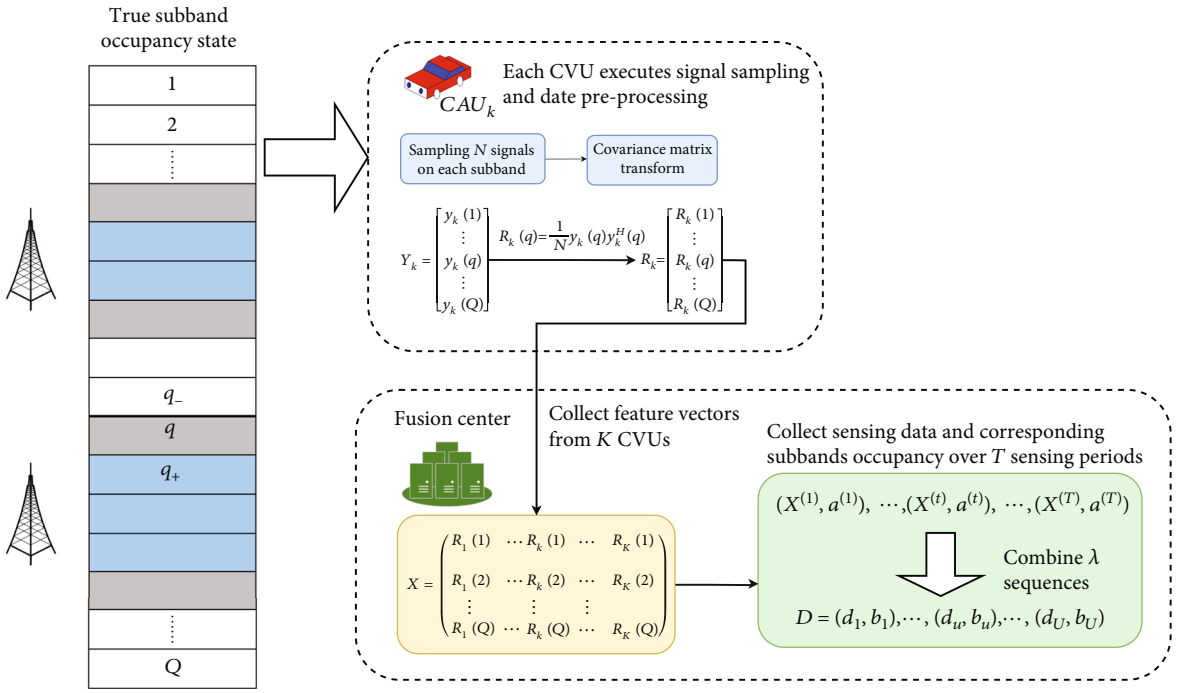

FIGURE 3: The procedure of data preprocessing.

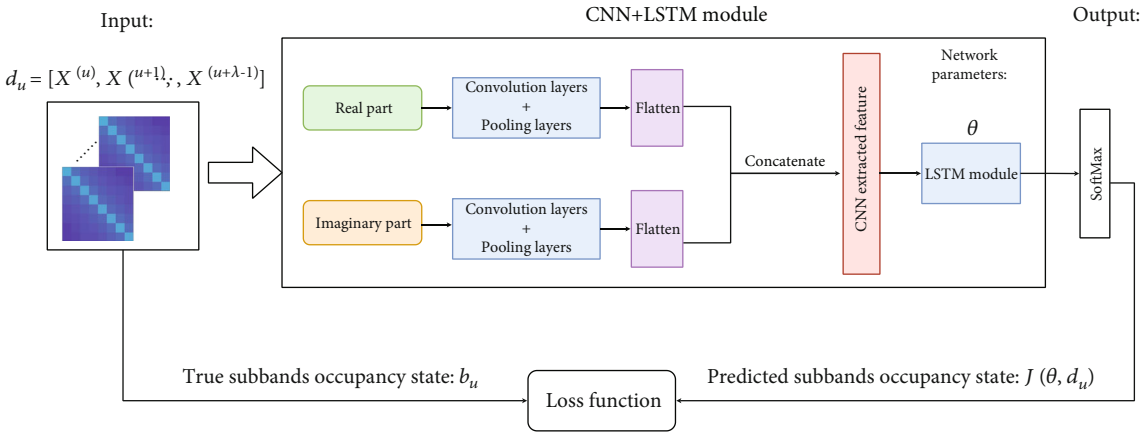

FIGURE 4: Network architecture of the proposed learning approach.

into two vectors and then concatenated. The CNN-extracted feature is viewed as the input into the following LSTM modules, which are responsible to exploit the time-dynamic correlations concealed in the series of sensing periods. At last, the output of the last LSTM cell is catenated with a dense layer to stand for the belief that the input corresponds to predicted subband occupancy.

After the formulation of the training input and the network structure, the next process is to design the loss function to train our proposed classifier. Given a training sample $<\mathbf{d}_u, \mathbf{b}_u>$, let $\mathcal{J}(\mathbf{d}_u; \boldsymbol{\theta})$ the prediction subband occupancy vector from the classifier, $\boldsymbol{\theta}$ be the classifier parameters. The categorical cross-entropy loss function, as formulated in equation (7), is employed to measure the difference between prediction value $\mathcal{J}(\mathbf{d}_u; \boldsymbol{\theta})$ and actual subband occupancy $\mathbf{b}_u$.

$$\mathcal{L}(\mathbf{d}_u, \mathbf{b}_u; \boldsymbol{\theta}) = -\sum_{q=1}^{Q} \mathbf{b}_u^{(q)} \log \mathbf{J}(\mathbf{d}_u; \boldsymbol{\theta})^{(q)} \tag{7}$$

Here, the $\mathbf{J}(\mathbf{d}_u; \boldsymbol{\theta})^{(q)}$ and $\mathbf{b}_u^{(q)}$ is the qth element of the actual/prediction subband occupancy vectors. In this way, the training loss on the collected training dataset can be denoted as $1/U \sum_u \mathcal{L}(\mathbf{d}_u, \mathbf{b}_u; \boldsymbol{\theta})$.

To minimize the loss value, the stochastic gradient descent (SGD) method and adaptive moment estimation (Adam) optimizer are adopted. The trained classifier can be evoked to recognize the subband occupancy pattern based on the matrix collected by all CAUs. In general, the training module should be activated when the network is initialized

Table 1: Network parameters of the proposed approach.

Network parameters	Value
Filters per conv layer	6
Filter size	16
Cells per LSTM layer	20
Neurons per flattened layer	128
Optimizer	Adam
Learning rate	0.003
Batch size	200

and periodically configured to catch up with the changing radio environment.

4. Numerical Analysis

4.1. Dataset Prerequisite. The PU signals are retrieved from the open-source RadioML2018.01a dataset [17], which includes 24 kinds of typically digital and analog modulated signals. For each class of modulation type, it contains 26 levels of SNR ranging from -20 to 30 dB with intervals of 2 dB. Each ⟨modulation, SNR⟩ pair is composed of 4096 examples and has a length of 1024 in-phase and quadrature (I/Q) complex-value per example. For simplicity, in this study, we limit the datasets to negative SNR, and seven linear modulations are simulated: BPSK, QPSK, 8PSK, 8QAM, 16QAM, 32QAM, and 64QAM. The entire dataset is partitioned into three halves for training, validating, and testing with a commonly used split ratio of 7 : 2 : 1.

4.2. Simulation Parameters. We conduct numerical experiments to corroborate the performance of the proposed method in a multiband cognitive vehicular network with $M = 3$ PUs using $Q = 16$ subbands for communication. The 3 PUs occupy 2, 3, and 4 consecutive subbands, respectively. On the channel model, Rayleigh fading is assumed with path-loss exponent $\alpha = 4$, the fading component $\nu = 1$. For the convenience of analysis, we set $P(H_1) = P(H_0) = 0.5$ about the PU activity pattern. During the network training process, we define 100 SGD iterations as an epoch, and after each epoch, we check the classification accuracy on the validation set and save the network parameters if the present sensing accuracy on the validation set is higher than that corresponding to the previous epochs. The network parameters determined through extensive cross-validation are detailed in Table 1. The Pytorch-based simulations are implemented on a computer with a CPU (Intel(R) Xeon(R) Gold 6134 M) and a GPU (NVIDIA Quadro P5000).

4.3. Results Evaluation. In this section, extensive simulation results are provided to demonstrate the performance superiority of the proposed approach. Also, the impact of key parameters such as SNR level and modulation scheme is investigated. For comparison, the benchmark methods include the traditional rule-based cooperative spectrum sensing methods, i.e., AND rule and the OR rule, two typically test-statistic methods such as energy detection (ED) [5], maximum-minimum eigenvalue (MME) [6], and another learning method of SVM, K-means, and covariance matrix CNN (CM-CNN) [8]. Note that all the baseline methods are introduced for narrowband spectrum sensing, and thus all the sensing results of them are obtained in each

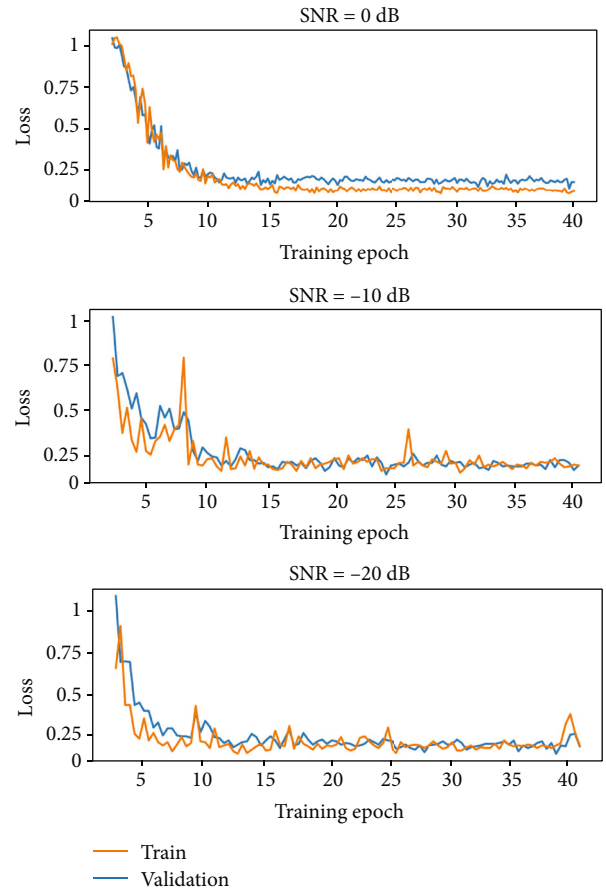

Figure 5: The loss value with training epoch iteration.

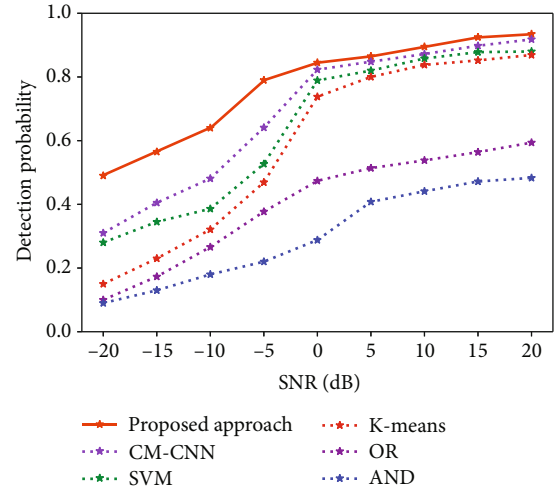

Figure 6: The detection probability of different methods.

Table 2: Complexity comparison of different spectrum sensing methods on offline training phase.

Metrics	Proposed	CM-CNN	SVM	K-means
FLOPs ($\times 10^7$)	1.79	1.21	0.71	0.027
Parameters ($\times 10^6$)	0.169	0.141	0.092	0.047
Training time (seconds)	170.5	138.01	63.2	40.9

Table 3: The prediction time (seconds) of different spectrum sensing methods in the online testing phase.

Proposed method	CM-CNN	SVM	K-means
0.057	0.083	0.12	0.07

subband separately. Each point in the simulation results is obtained by averaging 100 Monte Carlo realizations.

4.3.1. Loss function's Convergence with SNR Level. First, we evaluate the loss function's convergence behavior under different SNR levels. As shown in Figure 5, with the epoch of the model training, both training loss and validation loss are decreasing. In high SNR scenarios, the difference in extracted features from spectrum sensing data between idel subbands and occupied subbands is large, and therefore, the loss function shows quick convergence. With the decline of SNR, i.e., the wireless channel condition becomes worse; the inapparent difference in the subband state makes the classification task more difficult. The loss curve of the training process needs more iterative rounds to obtain statistical results. In addition, the loss value of the proposed approach is reduced smoothly in the training process and shows its superiority.

4.3.2. Spectrum Sensing Performance. The performance of the spectrum sensing algorithm is mainly evaluated by the detection probability. A higher detection probability signifies a better capability to protect PUs.Figure 6 shows the spectrum detection probability of the proposed approach and other compared methods under different SNR conditions. We can see that even under the condition of low SNRs, the detection probability of the proposed approach is still better than the others. Because the LSTM structure learns the time characteristics of historical sensing data, it obtains higher detection accuracy. It is depicted that the proposed approach can achieve the highest detection probability, and the detection probability of CM-CNN is slightly lower, closely approaching that of the proposed method. The SVM scheme is in the middle of performance. The detection probability of K-means is lower since it is an unsupervised learning diagram. The detection probability of the rule-based scheme is the lowest one due to the high difficulty of a full vote among all the SUs. It is also interesting that for the fusion rule, the detection probability of the AND-rule is a little lower than the OR-rule-based scheme. From these simulation results, we can see that the proposed classifier generally exhibits relatively superior performance and achieves the best performance among them.

4.3.3. Complexity Comparison. Finally, the specific complexity of different methods is compared. When analyzing the complexity of different methods, we consider three metrics in the offline training phase, namely, the required number of floating point operations (FLOPs), the total number of parameters, and the offline training time. The classifier training has usually been executed once in practice; therefore, we only evaluate the prediction delay in the online testing phase. Two tables (Tables 2 and 3) have been simulated to verify the superiority of the proposed method over others.

As a comparison, the proposed method demands the highest offline training duration among all the classifiers, and the additional FLOPs overhead is higher than other methods. For the classifier built on neural network methods, i.e., the proposed method and the CM-CNN method, they require a larger parameter number because of the cascaded structure of the neural network. Both the training duration and prediction delay for the K-means are founded to be normal. The proposed method shows the most rapid spectrum occupancy prediction. In addition, the SVM suffers from a very high prediction delay. It can be viewed that the proposed spectrum sensing approach can predict the spectrum state by mining the internal correlation of historical data, so the overall sensing time is greatly shortened. Another observation is reflected intuitively that with more sufficient training samples, it takes more effort to train the classifier to a satisfactory results.

5. Conclusion

In this work, we have studied the problem of multiband spectrum sensing in a cognitive vehicular network and developed a cooperative spectrum sensing algorithm based on the covariance matrix-aware CNN-LSTM. The proposed method can effectively learn the underlying dependence features across adjacent subbands and consecutive sensing periods to improve spectrum sensing performance. Numerical results demonstrated that the proposed method has a substantial performance advantage over other existing methods under noise uncertainty.

Data Availability

The data used in the simulation are retrieved from the open-source RadioML2018.01a dataset.

Conflicts of Interest

The authors declare that they have no conflicts of interest.

Acknowledgments

This project is supported by the Fundamental Research Funds for the Central Universities (2021CZ102).

References

[1] J. Li and B. J. Hu, "Quantized cooperative spectrum sensing in bandwidth-constrained cognitive V2X based on deep learning," *Electronics*, vol. 10, no. 11, p. 1315, 2021.

[2] R. D. Hippenstiel, *Detection Theory: Applications and Digital Signal Processing, [M.S. Thesis]*, CRC Press, 2017.

[3] W. A. Gardner, "Exploitation of spectral redundancy in cyclostationary signals," *IEEE Signal Processing Magazine*, vol. 8, no. 2, pp. 14–36, 1991.

[4] X. Zhang, R. Chai, and F. Gao, "Matched filter based spectrum sensing and power level detection for cognitive radio network," in *2014 IEEE Global Conference on Signal and Information Processing (GlobalSIP)*, pp. 1267–1270, Atlanta, GA, USA, 2014.

[5] F. F. Digham, M. -S. Alouini, and M. K. Simon, "On the energy detection of unknown signals over fading channels," *IEEE Transactions on Communications*, vol. 55, no. 1, pp. 21–24, 2007.

[6] Y. Zeng, C. L. Koh, and Y. C. Liang, "Maximum eigenvalue detection: theory and application," in *2008 IEEE international conference on communications*, pp. 4160–4164, Beijing, China, 2008.

[7] Y. Zeng and Y. C. Liang, "Spectrum-sensing algorithms for cognitive radio based on statistical covariances," *IEEE Transactions on Vehicular Technology*, vol. 58, no. 4, pp. 1804–1815, 2009.

[8] C. Liu, J. Wang, X. Liu, and Y.-C. Liang, "Deep CM-CNN for spectrum sensing in cognitive radio," *IEEE Journal on Selected Areas in Communications*, vol. 37, no. 10, pp. 2306–2321, 2019.

[9] Z. Chen, Y.-Q. Xu, H. Wang, and D. Guo, "Deep STFT-CNN for spectrum sensing in cognitive radio," *IEEE Communications Letters*, vol. 25, no. 3, pp. 864–868, 2021.

[10] J. Xie, J. Fang, C. Liu, and L. Yang, "Unsupervised deep spectrum sensing: a variational auto-encoder based approach," *IEEE Transactions on Vehicular Technology*, vol. 69, no. 5, pp. 5307–5319, 2020.

[11] K. Davaslioglu and Y. E. Sagduyu, "Generative adversarial learning for spectrum sensing," in *2018 IEEE international conference on communications (ICC)*, pp. 1–6, Kansas City, MO, USA, 2018.

[12] C. Wang, Y. Xu, Z. Chen, J. Tian, P. Cheng, and M. Li, "Adversarial learning-based spectrum sensing in cognitive radio," *IEEE Wireless Communications Letters*, vol. 11, no. 3, pp. 498–502, 2022.

[13] J. Xie, J. Fang, C. Liu, and X. Li, "Deep learning-based spectrum sensing in cognitive radio: a CNN-LSTM approach," *IEEE Communications Letters*, vol. 24, no. 10, pp. 2196–2200, 2020.

[14] J. Gao, X. Yi, C. Zhong, X. Chen, and Z. Zhang, "Deep learning for spectrum sensing," *IEEE Wireless Communications Letters*, vol. 8, no. 6, pp. 1727–1730, 2019.

[15] J. Zhang, Z.-Q. He, H. Rui, and X. Xu, "Multiband joint spectrum sensing via covariance matrix-aware convolutional neural network," *IEEE Communications Letters*, vol. 26, no. 7, pp. 1578–1582, 2022.

[16] N. E. West and T. O'shea, "Deep architectures for modulation recognition," in *2017 IEEE International Symposium on Dynamic Spectrum Access Networks (DySPAN)*, pp. 1–6, Baltimore, MD, USA, 2017.

[17] T. J. O'Shea, T. Roy, and T. C. Clancy, "Over-the-air deep learning based radio signal classification," *IEEE Journal of Selected Topics in Signal Processing*, vol. 12, no. 1, pp. 168–179, 2018.

Hindawi
Wireless Communications and Mobile Computing
Volume 2022, Article ID 4534692, 28 pages
https://doi.org/10.1155/2022/4534692

Research Article

Stability and Safety of Cooperative Adaptive Cruise Control Vehicular Platoon under Diverse Information Flow Topologies

Yulu Dai,[1] **Yuwei Yang**,[1] **Hongming Zhong**,[1] **Huijun Zuo**,[2] **and Qiang Zhang**[3]

[1]*School of Transportation, Southeast University, China*
[2]*Subunit 26 of Unit 96901 of PLA, Beijing, China*
[3]*Unit 61741 of PLA, Beijing, China*

Correspondence should be addressed to Yuwei Yang; yuweiy@seu.edu.cn

Received 6 July 2022; Accepted 1 August 2022; Published 21 August 2022

Academic Editor: Li Zhu

For the cooperative adaptive cruise control (CACC) vehicular platoon, apart from decentralized controllers, the dynamics of a platoon can be affected substantially by the information flow among connected and automated vehicles (CAVs). Existing research studies mainly focus on the stability analysis of platoons where CAVs only adopt the predecessor-following (PF) communication scheme; however, when CAVs "look" further ahead or behind than one vehicle, the stability of platoons might change. To this end, this study seeks to explore the stability and investigate the rear-end collision risk of CACC vehicular platoon under diverse information flow topologies. The research first comprehensively reviews typical information flow topologies for CAV platoons and platoon stability criteria for analyzing local and string stability of platoons. Moreover, the CACC longitudinal dynamic model is derived using the exact feedback linearization technique, which accommodates the inertial delay of powertrain dynamics. Accordingly, sufficient conditions of stability are mathematically derived to guarantee distributed frequency-domain-based control parameters. Simulation experiments are conducted to verify the correctness of derived sufficient stability conditions. The results show that platoons could better maintain stability with more vehicle information taken into consideration. However, when assessing the safety, it is found that the bidirectional type information flow topology would increase rear-end collision risk for CAV platoon. Further, the information flow topology of two-predecessor-leader following is the most recommended to enhance fully CAV platoon stability.

1. Introduction

Connected and automated vehicle (CAV) technologies, which incorporate communication technologies into autonomous systems to enable cooperative sensing and control [1, 2], are expected to improve traffic mobility, safety, and sustainability [3, 4]. A widely adopted method to achieve these purposes is adaptive cruise control (ACC), which is a vehicle-following control system that controls the speed in pace with the immediate preceding vehicles [5–7]. Moreover, the emergence of advanced communication (i.e., vehicle-to-everything (V2X) communication technology) has provided particularly promising for CAVs to receive additional information from other connected vehicles and could better form a platoon where CAVs travel as a string/chain to enhance traffic efficiency and stability. It has recently attracted extensive research interest (see [8–10] and the references therein).

From the viewpoint of control, CAV platoon is a controlled multiagent system where several vehicles are aimed at traveling at a common speed while keeping a safe distance within them. In this context, Cooperative Adaptive Cruise Control (CACC), which is an extension of ACC functionality, is recognized as an effective means to maintain stable and desired headways between adjacent vehicles [7, 11]. CACC has been modeled in a recent literature in different ways [12–15]. Among them, constant time headway (CTH) spacing policy is suggested to combine with CACC by many

studies, where the equilibrium spacing is defined as the speed multiplied by a predefined constant time headway plus a standstill spacing, since it is more robust to error propagation through traffic [16, 17].

On the other hand, for a CAV platoon, apart from decentralized controllers, the information flow among vehicles can significantly affect the dynamics, as well. In a platoon, agents exchange information (e.g., speed, intervehicle distance, and control inputs) with each other depending on how that information flows and a different communication scheme arises [18, 19]. The information flow topologies can describe the configuration of V2X communication links from one CAV to one or more CAVs in the platoon. Early-stage platoons primarily focus on predecessor following type which means that a vehicle can only obtain the information of its nearest front vehicles [20–23]. Under the V2X communication framework, more types of information flow topologies are proposed, such as the two-predecessors following type [24], the predecessor-leader following type [25], and the bidirectional type [26, 27]. For instance, an $H\infty$ controller synthesis approach is developed by [28] to guarantee platoon stability for platoons under one- and two-CAV look-ahead information flow topologies. Zheng et al. [18] study the relationship between information flow topology and the internal stability and scalability of CAV platoons moving in a rigid formation. However, to date, few studies have investigated the influence of different information flow topologies on CACC vehicular platoon stability.

The aim of stability analysis is to study how the perturbation of a leading vehicle evolves over time and space by assuming that vehicles travel on a single lane without overtaking. For the respective of CAV platoon, there exist two types of stability that have been defined in existing research: *local stability* and *string stability* [29, 30]. More specifically, if the distance gap and speed fluctuations of a single follower decrease with time, the CAVs are considered locally stable, while the platoon is string stable if local perturbations decay everywhere even in an arbitrarily long vehicle platoon. Hence, for a platoon to be stable, it is not enough just to satisfy the local stability but also to satisfy the string stability.

In conclusion, to the best of the authors' knowledge, the stability of a CAV platoon under diverse information flow topologies so far has not been considered before while most of the investigation is focused on the predecessor-following communication scheme. Moreover, few researches have evaluated the safety of CAV platoon under diverse information flow topologies. The main objective of this paper is to fill these gaps. To this aim, several main contributions are provided, each one corresponding to a different section.

This paper is organized as follows. Section 2 introduces different types of information flow topologies and the Cooperative Adaptive Cruise Control low for a CAV platoon. Section 3 provides the stability analysis of vehicular platoon under diverse information flow topologies. Numerical simulations are shown in Section 4, and the safety assessment is presented in Section 5. Concluding remarks and future research directions are described in the final section.

2. Diverse Information Flow Topologies for Cooperative Adaptive Cruise Control Vehicular Platoon

According to diverse information flow topologies, the control laws of the CAV platoon are diverse. In this section, the form of diverse information flow topologies and the corresponding CACC model would be elaborated on.

2.1. Diverse Information Flow Topologies. Due to V2X communication, CAVs can form platoons in the single-lane freeway sections where there is no cut-in/cutout behavior. The platoon consists of $N+1$ CAVs, as indicated in Figure 1, with a leading vehicle and N following vehicles. The platoon travels on a flat route and uses various information flow topologies. Figure 1 depicts six types of typical topologies as follows:

(1) Predecessor following (PF) topology

(2) Predecessor-leader following (PLF) topology

(3) Two-predecessor following (TPF) topology

(4) Bidirectional (BD) topology

(5) Bidirectional-leader (BDL) topology

(6) Two-predecessor-leader following (TPLF) topology

Specifically, for the leader following type (i.e., PLF, BDL, and TPLF), a leader with information broadcasting functions is indispensable; for the bidirectional type (i.e., BD and BDL), the controller can control utilizing information from both the preceding and following vehicles; for the two-predecessor type (i.e., TPF and TPLF), the controller can control utilizing information from both the two preceding vehicles. Furthermore, many more topologies are not included here for the sake of brevity, although they may all be examined using similar methods.

2.2. CAV Longitudinal Control with CACC. This section describes the formulation of the proposed distributed CAV longitudinal control. Assume that all CAVs in the platoon are of the same type. According to Zhou et al.'s [31] study, the CAV longitudinal control usually includes upper level and lower level controllers that govern CAVs to stay close and stable while compensating for vehicle longitudinal dynamics. The lower level controller prescribes the acceleration rate that can be realized after considering the vehicle longitudinal dynamics since the demanded acceleration may not be fully executed due to air drag force, gear position, etc.; meanwhile, the upper level controller, in particular, regulates a CAV to follow predefined equilibrium spacing at the same speed as the preceding vehicle via vehicle acceleration.

For the lower level controller, as suggested by Yi and Kwon [32], the generalized vehicle dynamic (GLVD) equation is leveraged to incorporate the nonlinear vehicle dynamics. The vehicle dynamics are specifically modeled using the first-order approximation as

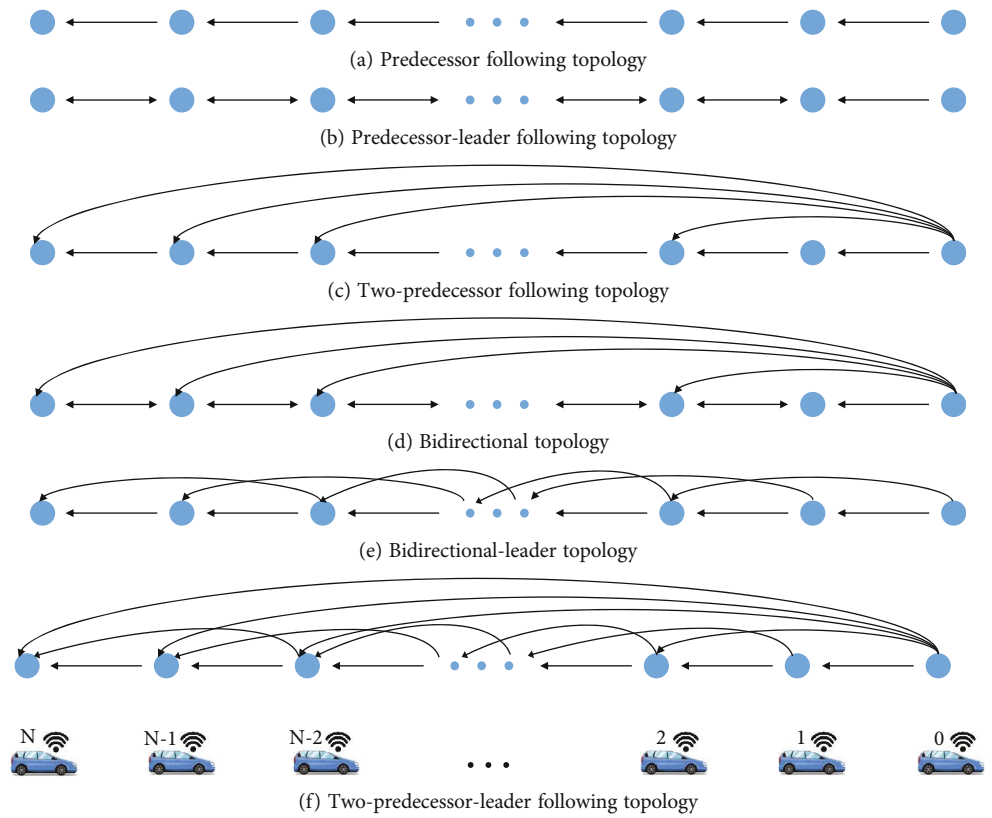

Figure 1: Typical information flow topologies for platoons.

$$\dot{a}_n(t) = -\frac{1}{T_L} a_n(t) + \frac{K_L}{T_L} u_n(t), \tag{1}$$

where K_L represents the ratio of demanded acceleration that can be realized (which ideally equals to 1) for CAVs, T_L is the time-lag for CAVs to realize the acceleration, $\dot{a}_n(t)$ is the jerk, $a_n(t)$ stands for the realized acceleration of CAV n at time t, and $u_n(t)$ is the demanded acceleration of CAV n at time t by the upper level controller, which also represents the control low of CAV n.

For the upper level controller, CACC combined with constant time gap policy which is shown to be more robust against disturbance propagation [17] is adopted. On the basis of the Society of Automotive Engineer (SAE) standard, the constant time gap policy is widely leveraged in CAV platoon control. According to the constant time gap policy [33], the equilibrium spacing is defined as

$$d_n^*(t) = v_n(t) \times \tau_n^* + l_n, \tag{2}$$

where $v_n(t)$ is the velocity of CAV n at time t, $d_n^*(t)$ is the target equilibrium spacing of CAV n at time t, τ_n^* presents the predefined constant time gap of CAV n, and l_n is the standstill spacing of CAV n. Moreover, the relationships between acceleration, velocity, and position of CAV n are defined as

$$a_n(t) = \dot{v}_n(t), \tag{3}$$

$$v_n(t) = \dot{p}_n(t), \tag{4}$$

where $p_n(t)$ is position of CAV n. Based on Equations (1)–(4), a 3rd-order state space model is derived for each CAV in the platoon with control input $u_n(t)$ as below:

$$\dot{x}_n(t) = A_n x_n(t) + B_n u_n(t), \tag{5}$$

where

$$A_n = \begin{bmatrix} 0 & 1 & 0 \\ 0 & 0 & 1 \\ 0 & 0 & -\frac{1}{T_L} \end{bmatrix}, B_n = \begin{bmatrix} 0 \\ 0 \\ \frac{K_L}{T_L} \end{bmatrix}, x_n(t) = [p_n(t), v_n(t), a_n(t)]^T. \tag{6}$$

Further, each controller can only use the information specified by $\mathbb{Q}_n$ which depends on the type of information flow topology applied to the platoon. The linear control law of CAV n (except the leading CAV) in the platoon is

$$\begin{aligned} u_n(t) = {} & k_1(p_{n-1}(t) - p_n(t) - d_n^*(t)) \\ & + k_2(v_{n-1}(t) - v_n(t)) + k_3(a_{n-1}(t) - a_n(t)) \\ & + \sum_{J \in \mathbb{Q}_n} \left[k_{Ja}(a_J(t) - a_n(t)) + k_{Jv}(v_J(t) - v_n(t)) \right], \end{aligned} \tag{7}$$

where $k_{\#}(\# = 1, 2, 3, Ja, Jv)$ is the control gain of the CACC and they all exceed zero. Except k_1, k_2, k_3, for the predecessor-leader following type, the control gains are written as k_{lv} and k_{la}; for two-predecessor following type, the control gains are written as k_{tv} and k_{ta}; for the bidirectional type, the control gains are written as k_{bv} and k_{ba}.

More specifically, based on Equation (7), the linear control law for CAV n under PF topology is

$$\begin{aligned} u_{n\_\mathrm{PF}}(t) = {} & k_1(p_{n-1}(t) - p_n(t) - d_n^*(t)) \\ & + k_2(v_{n-1}(t) - v_n(t)) + k_3(a_{n-1}(t) - a_n(t)). \end{aligned} \tag{8}$$

The linear control law for CAV n under PLF topology is described as

$$\begin{aligned} u_{n\_\mathrm{PLF}}(t) = {} & k_1(p_{n-1}(t) - p_n(t) - d_n^*(t)) \\ & + k_2(v_{n-1}(t) - v_n(t)) + k_3(a_{n-1}(t) - a_n(t)) \\ & + k_{lv}(v_0(t) - v_n(t)) + k_{la}(a_0(t) - a_n(t)). \end{aligned} \tag{9}$$

The linear control law for CAV n under TPF topology is described as

$$\begin{aligned} u_{n\_\mathrm{TPF}}(t) = {} & k_1(p_{n-1}(t) - p_n(t) - d_n^*(t)) + k_2(v_{n-1}(t) - v_n(t)) \\ & + k_3(a_{n-1}(t) - a_n(t)) + k_{tv}(v_{n-2}(t) - v_n(t)) \\ & + k_{ta}(a_{n-2}(t) - a_n(t)). \end{aligned} \tag{10}$$

The linear control law for CAV n under BD topology is written as

$$\begin{aligned} u_{n\_\mathrm{BD}}(t) = {} & k_1(p_{n-1}(t) - p_n(t) - d_n^*(t)) + k_2(v_{n-1}(t) - v_n(t)) \\ & + k_3(a_{n-1}(t) - a_n(t)) + k_{bv}(v_{n+1}(t) - v_n(t)) \\ & + k_{ba}(a_{n+1}(t) - a_n(t)). \end{aligned} \tag{11}$$

Likewise, the linear control law under TPLF topology is

$$\begin{aligned} u_{n\_\mathrm{TPLF}}(t) = {} & k_1(p_{n-1}(t) - p_n(t) - d_n^*(t)) + k_2(v_{n-1}(t) - v_n(t)) \\ & + k_3(a_{n-1}(t) - a_n(t)) + k_{lv}(v_0(t) - v_n(t)) \\ & + k_{la}(a_0(t) - a_n(t)) + k_{tv}(v_{n-2}(t) - v_n(t)) \\ & + k_{ta}(a_{n-2}(t) - a_n(t)) + k_{bv}(v_{n+1}(t) - v_n(t)) \\ & + k_{ba}(a_{n+1}(t) - a_n(t)). \end{aligned} \tag{12}$$

3. Stability Analysis of CACC Vehicular Platoon

As alluded, the control gains should be prudently selected to guarantee that the CACC vehicular platoon is stable. In this section, the theory of stability is concisely recalled from the control theory standpoint, and the stability of the CACC vehicular platoon under diverse information flow topologies is explored.

3.1. Preliminaries for Stability. In general, there are two typical categories of stability, which have been widely adopted for maintaining safety under perturbances while controlling vehicular platoon, i.e.,

(1) Local stability: a platoon following linear time-invariant dynamics is said to be locally stable concerning equilibrium state $x_{n,e}$ if and only if the closed-loop system has eigenvalues with strictly negative real parts [34].

(2) String stability: a platoon is said to be string stable if and only if the magnitude of a perturbance is not amplified for each leader-follower pair when propagating along the vehicular string [24, 25], as defined in

$$\|\mathscr{E}_1(s)\|_2 \geq \|\mathscr{E}_2(s)\|_2 \geq \|\mathscr{E}_3(s)\|_2 \geq \cdots \geq \|\mathscr{E}_n(s)\|_2, \tag{13}$$

where $\|.\|_2$ denotes the H_2 norm; $\mathscr{E}_n(s) \in \{a_n(s), v_n(s), p_{n-1}(s) - p_n(s) - d_n^*(t)\}$ and $\|\mathscr{E}_n(s)\|_2 = (\int_0^\infty |\mathscr{E}_n(wj)|^2 dw)^2$. $s = w$, where $w > 0$ represents frequency and j is the imaginary unit.

Local stability can guarantee each CAV can eliminate deviation from desired spacing and speed difference activated locally through a single vehicle by perturbances (deviation from equilibrium spacing, speed difference, or acceleration). Local stability is essential for any acceleration model since driver behavior is locally stable in reality. Furthermore, to satisfy the local stability, the sufficient condition by Hurwitz criterion [35] is given below.

3.1.1. Routh Hurwitz Stability Criterion. Given a polynomial, $p(s) = a_0 s^3 + a_1 s^2 + a_2 s + a_3$, where $a_0, a_1, a_2, a_3 \in \mathbb{R}$, $p(s)$ is stable if and only if $a_0, a_1, a_2, a_3 > 0$ and $a_1 a_2 > a_0 a_3$.

Unlike local stability, string stability considers how a small perturbation in the gap and speed of the leading vehicle influence the gap and speed of all the following vehicles in the platoon. Thus, the cohesion of the CAVs can be maintained, and the states of CAVs bounded can be kept by string stability. However, string stability is not always observed in empirical data. According to [7, 36, 37], string stability can also be divided into two kinds: strict string stability and head-to-tail string stability. Additionally, the detailed definition is as follows:

Definition 1 (strict string stability). A platoon system of a finite number of vehicles $N + 1$ is said to be strict string stable if satisfying for any sufficiently small perturbation input acting upon CAV 0, for any $n \in (0, N]$:

$$|F_n(s)|^2 = \frac{\|\mathscr{E}_n(s)\|_2}{\|\mathscr{E}_{n-1}(s)\|_2} \leq 1, \tag{14}$$

where $F_n(s)$ is the transfer function describing perturbance propagation between CAV $n-1$ and CAV n in the frequency domain.

Definition 2 (head-to-tail string stability). A platoon system of a finite number of vehicles $N+1$ is said to be head-to-tail string stable if satisfying for any sufficiently small perturbation input acting upon CAV 0, for any $n \in (0, N]$:

$$|G_n(s)|^2 = \frac{\|\mathscr{E}_n(s)\|_2}{\|\mathscr{E}_0(s)\|_2} \leq 1, \tag{15}$$

where $G_n(s)$ is the transfer function describing perturbance propagation from CAV 0 and CAV n in the frequency domain. Note that when $F_n(s) = 1$ and $G_n(s) = 1$, the CAV platoon is marginally H_2-norm string stable.

For perturbances in the form of velocity and acceleration, the transfer functions $F_n(s)$ and $G_n(s)$ are of the general form:

$$\begin{aligned} a_n(s) &= F_n(s)a_{n-1}(s), \\ v_n(s) &= F_n(s)v_{n-1}(s), \\ a_n(s) &= G_n(s)a_0(s), \\ v_n(s) &= G_n(s)v_0(s). \end{aligned} \tag{16}$$

Except for the velocity and acceleration oscillation, the spacing error can be obtained through Laplace Transformation:

$$s(p_{n-1}(s) - p_n(s)) = v_{n-1}(s) - v_n(s). \tag{17}$$

As there is no spacing error in the leading CAV, the transfer function is defined for other CAVs from the first following CAV to CAV n. Thus, the transfer functions of spacing error can be formulated as follows:

$$\begin{aligned} Fx_n(s) &= \frac{p_n(s) - p_{n-1}(s)}{p_{n-1}(s) - p_{n-2}(s)} \\ &= \frac{F_n(s)F_{n-1}(s) - F_{n-1}(s)}{F_{n-1}(s) - 1} \\ &= \frac{F_{n-1}(s)(F_n(s) - 1)}{F_{n-1}(s) - 1}, \end{aligned} \tag{18}$$

$$Gx_n(s) = \frac{p_n(s) - p_{n-1}(s)}{p_1(s) - p_0(s)} = \frac{G_n(s) - G_{n-1}(s)}{G_1(s) - 1}. \tag{19}$$

To address the string stability, based on [7], the worst cases, $F_{n-1}(s) = F_n(s) = 1$ and $G_{n-1}(s) = 1$, are taken into consideration to reduce the order in Equations (18) and (19). Therefore, we get

$$Fx_n(s) = F_{n-1}(s) = 1, \tag{20}$$

$$Gx_n(s) = \frac{G_n(s) - 1}{G_1(s) - 1} \left(\text{if } G_n(s) = G_1(s), Gx_n(s) = 1\right). \tag{21}$$

On the basis of Equations (20) and (21), aiming at analyzing the string stability of the CACC vehicular platoon under different information flow topologies, we can only concern the transfer functions $F_n(s)$ and $G_n(s)$.

3.2. Stability Analysis

3.2.1. Local Stability. Based on Routh Hurwitz stability criterion, local stability requires that the real-part of the Eigenvalue of matrix $A_{cn} = (A_n + B_nK)$ is less than zero, where $K = [k_1, k_2 + \sum_{J\in\mathbb{Q}_n} k_{Jv}, k_3 + \sum_{J\in\mathbb{Q}_n} k_{Ja}]$.

According to control law as Equation (7), we have

$$\begin{aligned} &\det(sI - A_{cn}) = 0 \\ \Longleftrightarrow &\frac{T_L}{K_L}s^3 + \left(\frac{1}{K_L} - k_3 - \sum_{J\in\mathbb{Q}_n} k_{Ja}\right)s^2 + \left(k_1\tau_n^* + k_2 + \sum_{J\in\mathbb{Q}_n} k_{Jv}\right)s + k_1 = 0. \end{aligned} \tag{22}$$

Hence, by applying the Hurwitz criterion, the CACC vehicular platoon is locally stable if the following inequalities are satisfied.

$$\frac{T_{iL}}{K_L} > 0, \tag{23a}$$

$$k_1 > 0, \tag{23b}$$

$$\frac{1}{K_L} - k_3 - \sum_{J\in\mathbb{Q}_n} k_{Ja} > 0, \tag{23c}$$

$$k_1\tau_n^* + k_2 + \sum_{J\in\mathbb{Q}_n} k_{Jv} > 0, \tag{23d}$$

$$\left(\frac{1}{K_L} - k_3 - \sum_{J\in\mathbb{Q}_n} k_{Ja}\right)\left(k_1\tau_n^* + k_2 + \sum_{J\in\mathbb{Q}_n} k_{Jv}\right) > \frac{T_L}{K_L}k_1. \tag{23e}$$

3.2.2. String Stability. Under diverse information flow topologies, the string stability needs to be analyzed separately.

(1) PF Topology. Based on Equation (8), for PF topology, the transfer function $F_n(s)$ is presented by

$$F_{n\_\mathrm{PF}}(s) = \frac{k_3s^2 + k_2s + k_1}{((T_L/K_L)s + (1/K_L) + k_3)s^2 + (k_1\tau_n^* + k_2)s + k_1}. \tag{24}$$

Building on Equations (14) and (24), the following sufficient condition for the H_2-norm string stability is shown:

$$\left\|F_{n\_\mathrm{PF}}(s)\right\|_2 = \sup\left|\frac{-k_3w^2 + k_2wj + k_1}{-((T_L/K_L)wj + (1/K_L) + k_3)w^2 + (k_1\tau_n^* + k_2)wj + k_1}\right| \leq 1. \tag{25}$$

Hence, the CACC vehicular platoon under PF topology is strict string stable if the following inequalities are satisfied.

$$\frac{1}{K_L^2} + \frac{2k_3}{K_L} - \frac{2T_L}{K_L}(k_1\tau_n^* + k_2) + k_3^2 - k_1^2 \geq 0, \tag{26a}$$

$$k_1\tau_n^{*2} + 2k_2\tau_n^* - \frac{2}{K_L} \geq 0, \tag{26b}$$

$$\frac{T_L}{K_L} \geq 0. \tag{26c}$$

Under PF topology, the head-to-tail string stability can be written as

$$G_{n\_PF}(s) = \prod_{i=1}^{n} F_{n\_PF}(s). \tag{27}$$

When $\|F_{n\_PF}(s)\|_2 \leq 1$, $\|G_{n\_PF}(s)\|_2$ is not greater than 1. In conclusion, the CAV platoon under PF topology is string stable if the inequations in Equations (26a), (26b), and (26c) are satisfied.

(2) PLF Topology. Under PLF topology, based on Equation (9), the first following CAV could be affected by the leading CAV, and the transfer function $G_{1\_\mathrm{PLF}}(s)$ is written as

$$G_{1\_\mathrm{PLF}}(s) = \frac{a_1(s)}{a_0(s)} = \frac{(k_3 s^2 + k_2 s + k_1) + (k_{lv} s + k_{la} s^2)}{((T_L/K_L)s + (1/K_L) + k_3 + k_{la})s^2 + (k_1 \tau_n^* + k_2 + k_{lv})s + k_1}. \tag{28}$$

Differently, the second following CAV could be affected by both its predecessor and the leader. Consequently, through substituting Equation (28), its transfer function is formulated as

$$G_{2\_\mathrm{PLF}}(s) = \frac{a_2(s)}{a_0(s)} = \frac{G_{1\_\mathrm{PLF}}(s)(k_3 s^2 + k_2 s + k_1) + (k_{lv} s + k_{la} s^2)}{((T_L/K_L)s + (1/K_L) + k_3 + k_{la})s^2 + (k_1 \tau_n^* + k_2 + k_{lv})s + k_1}. \tag{29}$$

For the rest following CAV n, the transfer function can be obtained by induction:

$$G_{n\_\mathrm{PLF}}(s) = \frac{G_{n-1\_\mathrm{PLF}}(s)(k_3 s^2 + k_2 s + k_1) + (k_{lv} s + k_{la} s^2)}{((T_L/K_L)s + (1/K_L) + k_3 + k_{la})s^2 + (k_1 \tau_n^* + k_2 + k_{lv})s + k_1}. \tag{30}$$

Nevertheless, the above Equation (30), is a high-order transfer function which is too complicated to be analyzed directly. In this way, we have the following formulation assuming the worst case, $G_{n-1\_\mathrm{PLF}}(s) = 1$:

$$G_{n\_\mathrm{PLF}}(s) = \frac{k_3 s^2 + k_2 s + k_1 + k_{lv} s + k_{la} s^2}{((T_L/K_L)s + (1/K_L) + k_3 + k_{la})s^2 + (k_1 \tau_n^* + k_2 + k_{lv})s + k_1}. \tag{31}$$

Hence, the CACC vehicular platoon under PLF topology is head-to-tail string stable if the following inequalities are satisfied:

$$\frac{1}{K_L^2} + \frac{2(k_3 + k_{la})}{K_L} - \frac{2T_L}{K_L}(k_1 \tau_n^* + k_2 + k_{lv}) + (k_3 + k_{la})^2 - k_1^2 \geq 0, \tag{32a}$$

$$k_1 \tau_n^{*2} + 2(k_2 + k_{lv})\tau_n^* - \frac{2}{K_L} \geq 0, \tag{32b}$$

$$\frac{T_L}{K_L} \geq 0. \tag{32c}$$

Comparing Equations (32a) and (32b) with Equations (26a) and (26b), it can be found that the value ranges of k_1, k_2, k_3 (i.e., the stable region) under PLF topology are greater than that under PF topology, since CAVs could obtain more information (i.e., the leading vehicle information) under PLF topology than under PF topology.

Similarly, the transfer function F_{n_PLF} is presented as

$$F_{n\_\mathrm{PLF}}(s) = \frac{k_1 + k_2 s + k_3 s^2 + (k_{lv} s + k_{la} s^2 / G_{n-1\_\mathrm{PLF}}(s))}{((T_L/K_L)s + (1/K_L) + k_3 + k_{la})s^2 + (k_1 \tau_n^* + k_2 + k_{lv})s + k_1}. \tag{33}$$

Consider the worst case:

$$F_{n\_\mathrm{PLF}}(s) = G_{n\_\mathrm{PLF}}(s) = \frac{k_3 s^2 + k_2 s + k_1 + k_{lv} s + k_{la} s^2}{((T_L/K_L)s + (1/K_L) + k_3 + k_{la})s^2 + (k_1 \tau_n^* + k_2 + k_{lv})s + k_1}. \tag{34}$$

In brief, the CACC vehicular platoon under PLF topology is string stable if the inequations in Equations (32a), (32b), and (32c) are satisfied.

(3) TPF Topology. Correspondingly, under TPF topology, based on Equation (10), expressions of the transfer function are

$$G_{n\_\mathrm{TPF}}(s) = \frac{G_{n-1\_\mathrm{TPF}}(s)(k_1 + k_2 s + k_3 s^2) + (k_{tv} s + k_{ta} s^2) G_{n-2\_\mathrm{TPF}}(s)}{((T_L/K_L)s + (1/K_L) + k_3 + k_{ta})s^2 + (k_1 \tau_n^* + k_2 + k_{tv})s + k_1},$$
$$F_{n\_\mathrm{TPF}}(s) = \frac{k_1 + k_2 s + k_3 s^2 + ((k_{tv} s + k_{ta} s^2)/F_{n-1\_\mathrm{TPF}}(s))}{((T_L/K_L)s + (1/K_L) + k_{ta})s^2 + (k_1 \tau_n^* + k_2 + k_{tv})s + k_1}. \tag{35}$$

Considering the worst case, the CACC vehicular platoon under TPF topology is string stable if the following inequations are satisfied. Compared with the stable region under PF topology, the stable region under TPF topology is larger.

$$\frac{1}{K_L^2} + \frac{2(k_3 + k_{ta})}{K_L} - \frac{2T_L}{K_L}(k_1 \tau_n^* + k_2 + k_{tv}) + (k_3 + k_{ta})^2 - k_1^2 \geq 0, \tag{36a}$$

$$k_1 \tau_n^{*2} + 2(k_2 + k_{tv})\tau_n^* - \frac{2}{K_L} \geq 0, \tag{36b}$$

$$\frac{T_L}{K_L} \geq 0. \tag{36c}$$

(4) BD Topology. Under BD topology, based on Equation (11), the transfer function can be written as

$$F_{n\_\mathrm{BD}}(s) = \frac{k_1 + k_2 s + k_3 s^2}{((T_L/K_L)s + (1/K_L) + k_3 + k_{ba})s^2 + (k_1\tau_n^* + k_2 + k_{bv})s + k_1 - F_{n+1\_\mathrm{BD}}(s)(k_{ba}s^2 + k_{bv}s)},$$
$$G_{n\_\mathrm{BD}}(s) = \frac{G_{n-1\_\mathrm{BD}}(s)\left(k_1 + k_2 s + k_3 s^2\right)}{((T_L/K_L)s + (1/K_L) + k_3 + k_{ba})s^2 + (k_1\tau_n^* + k_2 + k_{bv})s + k_1 - F_{n+1_{\mathrm{BD}}}(s)(k_{ba}s^2 + k_{bv}s)}. \tag{37}$$

When $F_{n+1\_\mathrm{BD}}(s) = 1$, $F_{n\_\mathrm{BD}}(s) = F_{n\_\mathrm{PF}}(s)$. However, when $F_{n+1\_\mathrm{BD}}(s) \neq 1$, the CACC vehicular platoon under BD topology is string stable if

$$\frac{1}{K_L^2} + \frac{2\left(k_3 + \left\|1 - F_{n+1_{BD}}(s)\right\|_2 k_{ba}\right)}{K_L} - \frac{2T_L}{K_L}\left(k_1\tau_n^* + k_2 + \left\|1 - F_{n+1_{BD}}(s)\right\|_2 k_{bv}\right) + \left(k_3 + \left\|1 - F_{n+1_{\mathrm{BD}}}(s)\right\|_2 k_{ba}\right)^2 - k_1^2 \geq 0, \tag{38a}$$

$$k_1\tau_n^{*2} + 2\left(k_2 + \left\|1 - F_{n+1_{\mathrm{BD}}}(s)\right\|_2 k_{bv}\right)\tau_n^* - \frac{2}{K_L} \geq 0, \tag{38b}$$

$$\frac{T_L}{K_L} \geq 0. \tag{38c}$$

As a matter of fact, we set the CACC controllers to make $\|F_{n+1\_\mathrm{BD}}(s)\|_2 < 1$. Thus, $\|F_{n\_\mathrm{BD}}(s)\|_2 < \|F_{n\_\mathrm{PF}}(s)\|_2$, and $\|G_{n\_\mathrm{BD}}(s)\|_2 < \|G_{n\_\mathrm{PF}}(s)\|_2$. The stable region for BD topology is larger than the stable region for PF topology.

(5) BDL Topology. Based on PLF topology and BD topology, under BDL topology, based on Equation (12), the transfer function of $F_{n\_\mathrm{BDL}}(s)$ and $G_{n\_\mathrm{BDL}}(s)$ can be written as

$$F_{n\_\mathrm{BDL}}(s) = \frac{k_1 + k_2 s + k_3 s^2 + \left(\left(k_{lv}s + k_{la}s^2\right)/G_{n-1\_\mathrm{BDL}}(s)\right)}{((T_L/K_L)s + (1/K_L) + k_3 + k_{la} + k_{ba})s^2 + (k_1\tau_n^* + k_2 + k_{lv} + k_{bv})s + k_1 - F_{n+1\_\mathrm{BDL}}(s)(k_{ba}s^2 + k_{bv}s)}, \tag{39}$$

$$G_{n\_\mathrm{BDL}}(s) = \frac{G_{n-1\_\mathrm{BDL}}(s)\left(k_3 s^2 + k_2 s + k_1\right) + \left(k_{lv}s + k_{la}s^2\right)}{((T_L/K_L)s + (1/K_L) + k_3 + k_{la} + k_{ba})s^2 + (k_1\tau_n^* + k_2 + k_{lv} + k_{bv})s + k_1 - F_{n+1\_\mathrm{BDL}}(s)(k_{ba}s^2 + k_{bv}s)}. \tag{40}$$

In addition, when $F_{n+1\_\mathrm{BDL}}(s) = 1$, $F_{n\_\mathrm{BDL}}(s) = F_{n\_\mathrm{PLF}}(s)$; when $F_{n+1\_\mathrm{BDL}}(s) \neq 1$, the CACC vehicular platoon under BDL topology is string stable if inequations in Equations (41a), (41b), and (41c) are met. Therefore, the stable region for BDL topology is larger than the stable region for PF topology and even larger than the stable region for PLF topology.

$$\frac{1}{K_L^2} + \frac{2\left(k_3 + + k_{la} + \left\|1 - F_{n+1\_\mathrm{BDL}}(s)\right\|_2 k_{ba}\right)}{K_L} - \frac{2T_L}{K_L}\left(k_1\tau_n^* + k_2 + k_{lv} + \left\|1 - F_{n+1_{\mathrm{BDL}}}(s)\right\|_2 k_{bv}\right) + \left(k_3 + k_{la} + \left\|1 - F_{n+1_{\mathrm{BDL}}}(s)\right\|_2 k_{ba}\right)^2 - k_1^2 \geq 0, \tag{41a}$$

$$k_1\tau_n^{*2} + 2\left(k_2 + k_{lv} + \left\|1 - F_{n+1_{\mathrm{BDL}}}(s)\right\|_2 k_{bv}\right)\tau_n^* - \frac{2}{K_L} \geq 0, \tag{41b}$$

$$\frac{T_L}{K_L} \geq 0. \tag{41c}$$

(6) TPLF Topology. Likewise, under TPLF topology, based on Equation (13), the transfer functions are presented as

$$G_{n\_\mathrm{TPLF}}(s) = \frac{G_{n-1\_\mathrm{TPLF}}(s)\left(k_1 + k_2 s + k_3 s^2\right) + G_{n-2\_\mathrm{TPLF}}(s)\left(k_{tv} s + k_{ta} s^2\right) + \left(k_{lv} s + k_{la} s^2\right)}{((T_L/K_L)s + (1/K_L) + k_3 + k_{ta} + k_{la})s^2 + (k_1\tau_n^* + k_2 + k_{tv} + k_{lv})s + k_1},$$
$$F_{n\_\mathrm{TPLF}}(s) = \frac{k_1 + k_2 s + k_3 s^2 + \left(\left(k_{tv} s + k_{ta} s^2\right)/F_{n-1\_\mathrm{TPLF}}(s)\right) + \left(\left(k_{lv} s + k_{la} s^2\right)/G_{n-1\_\mathrm{TPLF}}(s)\right)}{((T_L/K_L)s + (1/K_L) + k_3 + k_{ta} + k_{la})s^2 + (k_1\tau_n^* + k_2 + k_{tv} + k_{lv})s + k_1}. \tag{42}$$

With the worst case, the CACC vehicular platoon under TPLF topology is string stable if

$$\frac{1}{K_L^2} + \frac{2(k_3 + k_{la} + k_{ta})}{K_L} - \frac{2T_L}{K_L}(k_1\tau_n^* + k_2 + k_{lv} + k_{tv}) + (k_3 + k_{la} + k_{ta})^2 - k_1^2 \geq 0, \tag{43a}$$

$$k_1\tau_n^{*2} + 2(k_2 + k_{tv} + k_{lv})\tau_n^* - \frac{2}{K_L} \geq 0, \tag{43b}$$

$$\frac{T_L}{K_L} \geq 0. \tag{43c}$$

On the whole, under diverse information flow topologies, with more information a CAV obtains, the larger stable region the platoon system has and the CAV platoon is easier to control for maintaining stability. However, according to Zheng et al.'s study [18], under bidirectional topology, the scalability of CAV platoon will be affected. Moreover, for a pure CAV platoon, the perturbances are often applied to the leading vehicle instead of internal CAVs. Hence, the leader-type information flow topology can play an important role in enhancing stability. In this study, the information flow topology of TPLF provides the largest stable region for CAV platoon control.

4. Numerical Simulation

Numerical simulations are conducted to illustrate the main results. The parameter setting for the CACC vehicular platoon is given in Table 1, according to the existing studies [28, 31]. Unless otherwise specified, these parameters would not change. Since CAVs under PF topology are simplest for control and receive the least information, the CAV performance under PF topology is set as the baseline.

Based on the parameter setting, Figure 2 illustrates the regions of feedback gains for different information flow topologies to satisfy the local and string stability. The plots suggest empirically that with more information given to the CAV, the stable region will be larger, which supports the stability analysis results in Section 3.

To further verify the theoretical results presented in Section 3, we conduct two simulation scenarios on the CACC vehicular platoon: with simulated perturbation and with the human-driven vehicle trajectory. In both scenarios, we consider a CAV platoon with 11 identical CAVs (1 leader and 10 followers) interconnected by the six information flow topologies shown in Figure 1. In addition, the CAV length is equal to 3 m and the control gains k_1, k_2, k_3 are set as 2, 2, and 1, respectively.

4.1. Scenario I: With Simulated Perturbation. In this case, the initial state of the leading CAV is set as $p_0(t) = 0$, $v_0(t) = 20$ m/s and the desired trajectory is given by

$$v_n(t) = \begin{cases} 20\ \mathrm{m/s}, & t \leq 5s, \\ 20 + 2t, & 5s < t \leq 9s, \\ 30\ \mathrm{m/s}, & t > 9s. \end{cases} \tag{44}$$

The initial state of the platoon is set as the desired state; i.e., the initial spacing errors and velocity errors are all equal to 0. Figures 3–5 demonstrate distance gap, velocity gap, and acceleration under different information flow topologies. It is noted that under different information flow topologies, when the platoon is stable, the maximum values of velocity gap between CAV 9 and CAV 10 are lower than the maximum values of velocity gap between other CAVs. Furthermore, under different information flow topologies, the maximum values of acceleration of the last CAV in a stable platoon are lower than the maximum values of acceleration of other CAVs in the platoon. Particularly, the last CAVs in the platoon under the TPLF topology are of the smallest changes in the amplitude of acceleration as well as the amplitude of velocity gap, compared with other information flow topologies. Meanwhile, platoons under the leader type topology could better keep stability than other types for it assists communication among the whole platoon.

4.2. Scenario II: With Human-Driven Vehicle Trajectories from NGSIM. To explore CAV platoon stability in a more realistic situation, simulation experiments embedded with field data are carried out field. Hence, two sets of trajectory data of the real-world vehicle that experienced stop-and-go perturbances are obtained from the NGSIM dataset [38, 39]. The leading vehicles adopt the data of vehicle #1992 in Lane 2 from 4:00 p.m. to 4:15 p.m. on April 13, 2005, for Interstate 80 (i.e., I-80) in Emeryville, and the data of vehicle #1635 in Lane 1 from 7:50 a.m. to 8:35 a.m. on June 15, 2005, for US101 freeway (i.e., US101) in Los Angeles, whose dynamic statuses are illustrated in Figures 6 and 7. Note that, due to the noise in the acceleration data, the data is handled via a low-pass filter with the lower bound of 0.5 Hz.

Table 1: Default value setting for the experimental design.

Parameters	Value
K_L	1
T_L	0.45 s
τ_n^*	0.5 s
l_n	5 m
$F_{n+1\_\mathrm{BDL}}(s), F_{n+1\_\mathrm{BD}}(s)$	0.8
k_{la}, k_{ta}, k_{ba}	0.5
k_{lv}, k_{tv}, k_{bv}	1

Figures 8–10 demonstrate distance gap, velocity gap, and acceleration under different information flow topologies with vehicle #1992 as the leading vehicle. Among Figures 8–10, the amplitudes of distance gap and velocity gap as well as the acceleration of PF topology are larger than those of other information flow topologies. Consistent with the above result, TPLF holds the best stability among the six topologies.

Figures 11–13 show distance gap, velocity gap, and acceleration under different information flow topologies with vehicle #1635 as the leading vehicle. Similar to the case with vehicle #1992 as the leading vehicle, all topologies could offer stability for platoons and TPLF works best.

From the above simulations, we can find that when stable conditions are satisfied, with more information a CAV obtains, the CAV platoon is more stable under perturbances, since the larger stable region means the system has a significant ability to resist the perturbances. In addition, we also find that the leader type could better maintain stability than other types. The reason is that the perturbances are applied to the leader in the platoon in this study.

4.3. Sensitivity Analysis. In order to explore the influence of inertial delay of powertrain dynamics on the stability of CACC vehicular platoon under diverse information flow topologies, simulation analyses are conducted. Based on the parameters of K_L and T_L setting, Figures 14–17 illustrate stable regions of control gains for information flow topologies to satisfy the platoons' local and string stability.

Comparing the Figure 2 ($T_L = 0.45$ s) with Figure 14 ($T_L = 0.6$ s) as well as Figure 15 ($T_L = 0.3$ s), it can be found that with the same K_L (setting $K_L = 1$), the lesser the actuation lag, the more stable a CACC vehicular platoon is. Besides, the changes in stable regions under diverse information flow topologies accord with the theoretical analysis results in Section 3.

Then numerical simulations of three K_L values were carried out based on the stability analysis in Section 3.2. It should be emphasized that the value of K_L cannot exceed one. With the same T_L (setting $T_L = 0.45$ s), comparing the Figure 2 ($K_L = 1$) with Figure 16 ($K_L = 0.9$) as well as Figure 17 ($K_L = 0.8$), the larger the ratio of demanded acceleration that can be realized, the more stable a CACC vehicular platoon is.

5. Safety Assessment

To thoroughly assess the risk probability of CAVs, Time-to-collision (TTC), the modified Time Integrated Time-to-collision (TIT) and the Time Exposed Time-to-collision (TET) are employed in this study. TTC is defined as the time required for two vehicles to collide if they keep their current velocity on the same path [40]:

$$\mathrm{TTC}_n(k) = \begin{cases} \dfrac{p_{n-1}(k) - p_n(k) - l}{v_n(k) - v_{n-1}(k)}, & \text{if } v_n(k) > v_{n-1}(k), \\ \infty, & \text{if } v_n(k) \le v_{n-1}(k). \end{cases} \tag{45}$$

Herein, a larger TTC indicates a safer condition. It is worth mentioning that minimum TTC could only demonstrate the most dangerous degree of vehicles while ignoring the overall duration. Hence, we use minimum TTC value to evaluate the danger degree during moving.

Both TET and TIT are aggregated indexes from TTC for safety evaluation. Concretely, the expression of TIT and TET can be presented as [41]

$$\begin{aligned} \mathrm{TIT}(k) &= \sum_{k=1}^{N} \left(\frac{1}{\mathrm{TTC}_k(k)} - \frac{1}{\mathrm{TTC}^*} \right) \Delta t, \quad \forall 0 < \mathrm{TTC}_i(t) \le \mathrm{TTC}^*, \\ \mathrm{TIT} &= \sum_{t=0}^{T} \mathrm{TIT}(k), \\ \mathrm{TET}(k) &= \sum_{k=1}^{N} \delta_k \bullet \Delta \mathrm{t}, \delta_k = \begin{cases} 1, & \forall 0 < \mathrm{TTC}_i(k) \le \mathrm{TTC}^*, \\ 0, & \text{else}, \end{cases} \\ \mathrm{TET} &= \sum_{k=0}^{T} \mathrm{TET}(k), \end{aligned} \tag{46}$$

where TTC^* is the threshold of TTC value and Δt stands for the sampling time. Furthermore, a larger TIT/TET indicates a more dangerous condition. TET could present the rear-end collision risk, and TIT shows the duration of having the risk of rear-end collision over the whole operation.

Aiming at further evaluating the safety of different information flow topologies, we select three more real-world single vehicles from NGSIM I-80 dataset randomly: Vehicle #12, #391, and #2385, as the leading vehicle. The trajectories of these vehicles are shown in Figure 18, and the entire traveling time for each vehicle is 70.5 s, 37.1 s, and 34.5 s, respectively.

The results of minimum TTC, TIT, and TET values for the CACC vehicular platoons under diverse information flow topologies with real-world vehicle trajectories described in Section 4 and Figure 18 are demonstrated in Table 2, where $\Delta t = 0.1$s, $\tau_n^* = 0.5$ s (then, the desired intervehicular distance can be calculated by Equation (2) at each sampling time), and all CAVs are in equilibrium at the initial time

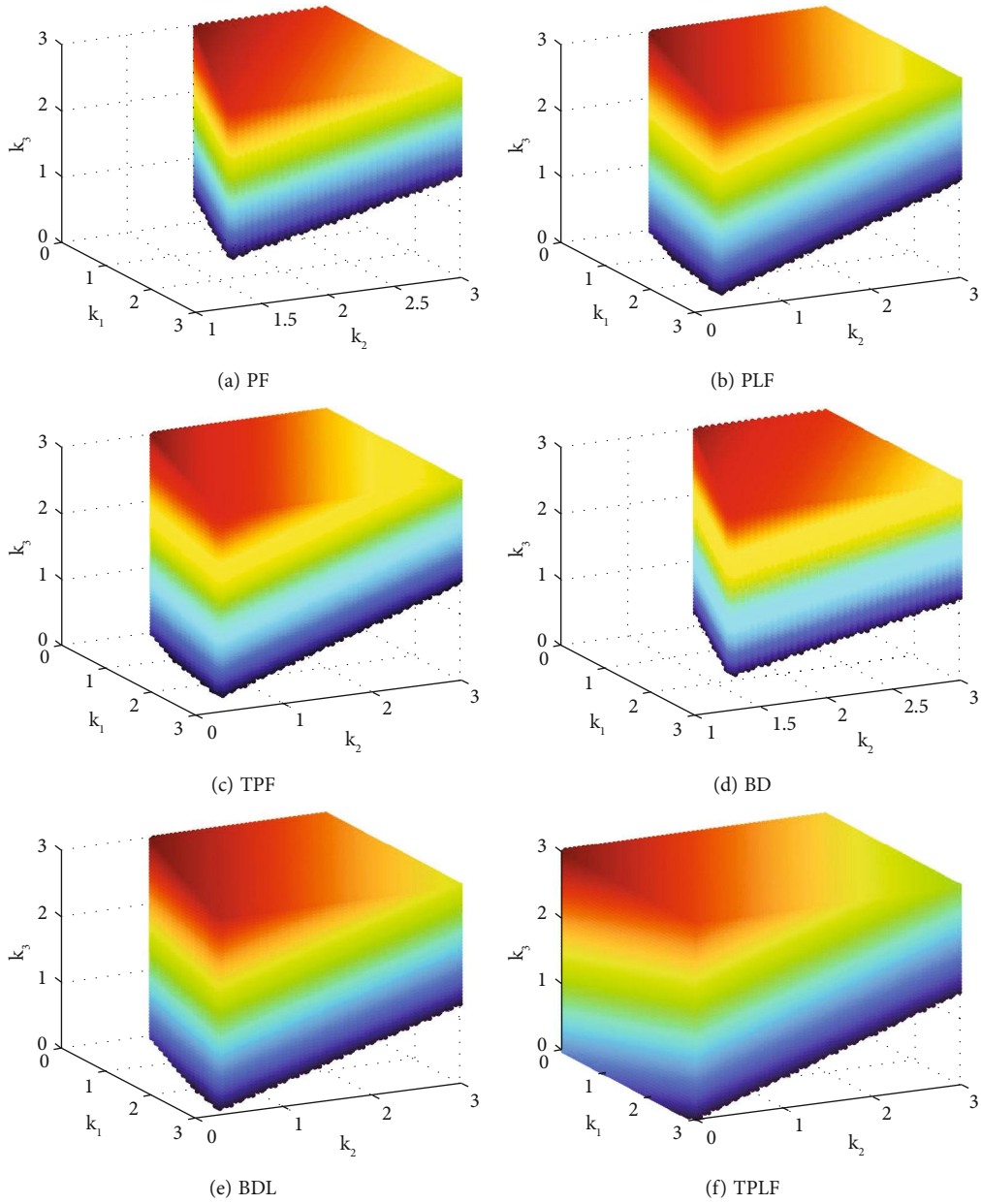

Figure 2: Stable region of feedback gains for diverse information flow topologies ($K_L = 1, T_L = 0.45s$).

with the same velocity as the leading vehicle. Moreover, the threshold of TTC value (i.e., TTC*) is also set as 0.5 s, which is equal to the desired time headway.

The results in Table 2 suggest the following: (1) from the aspect of minimum TTC, with more information, CAV platoon could better reduce the risk of rear-end collisions. However, in general, there is less impact of information flow topologies on minimum TTC; (2) from the aspect of TET, predecessor-leader following type (i.e., PLF, BDL, and TPLF) could better maintain safety for CAV platoons. Meanwhile, the two-predecessor type topologies perform better than the bidirectional type topologies since the TET values of CAV platoon under TPF topology are larger than those under BD topology and the TET values of CAV platoon under TPLF topology are larger than those under BDL topology; (3) from the aspect of TIT, the bidirectional type topologies could bring adverse impact on reducing the risk of rear-end collision and predecessor-leader following type could also enhance the CAV platoon safety. In all cases, the TIT values under BD topology are larger than that under PF topology, and the TIT values under BDL are larger than that under PLF topology. It is worth noting that the CAV under TPLF topology could reduce TIT by half compared with the CAV under PF topology. Therefore, among the six information flow topologies, TPLF is the most recommended to enhance both stability and safety.

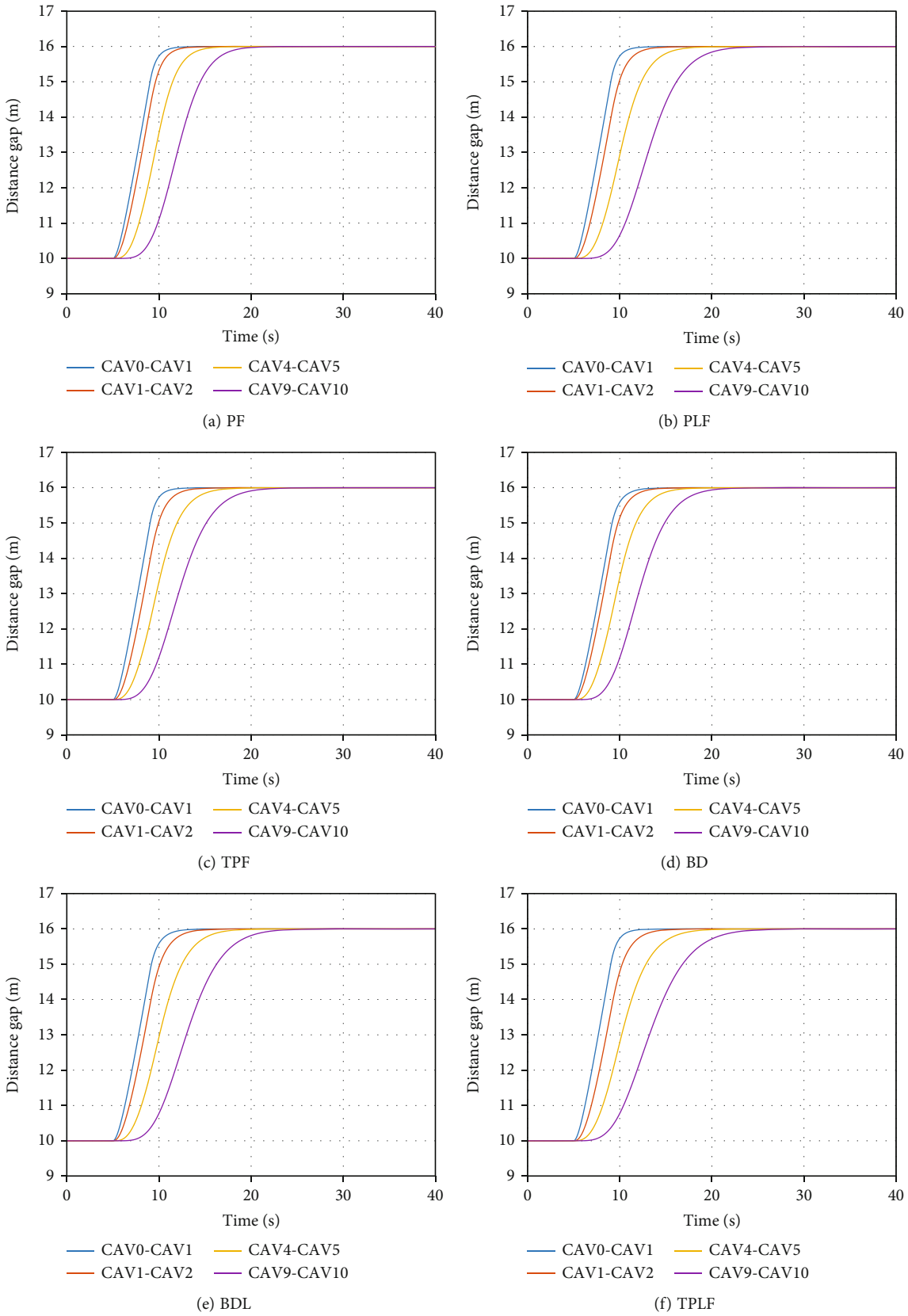

Figure 3: Platoon distance gap with simulated perturbation under diverse information flow topologies.

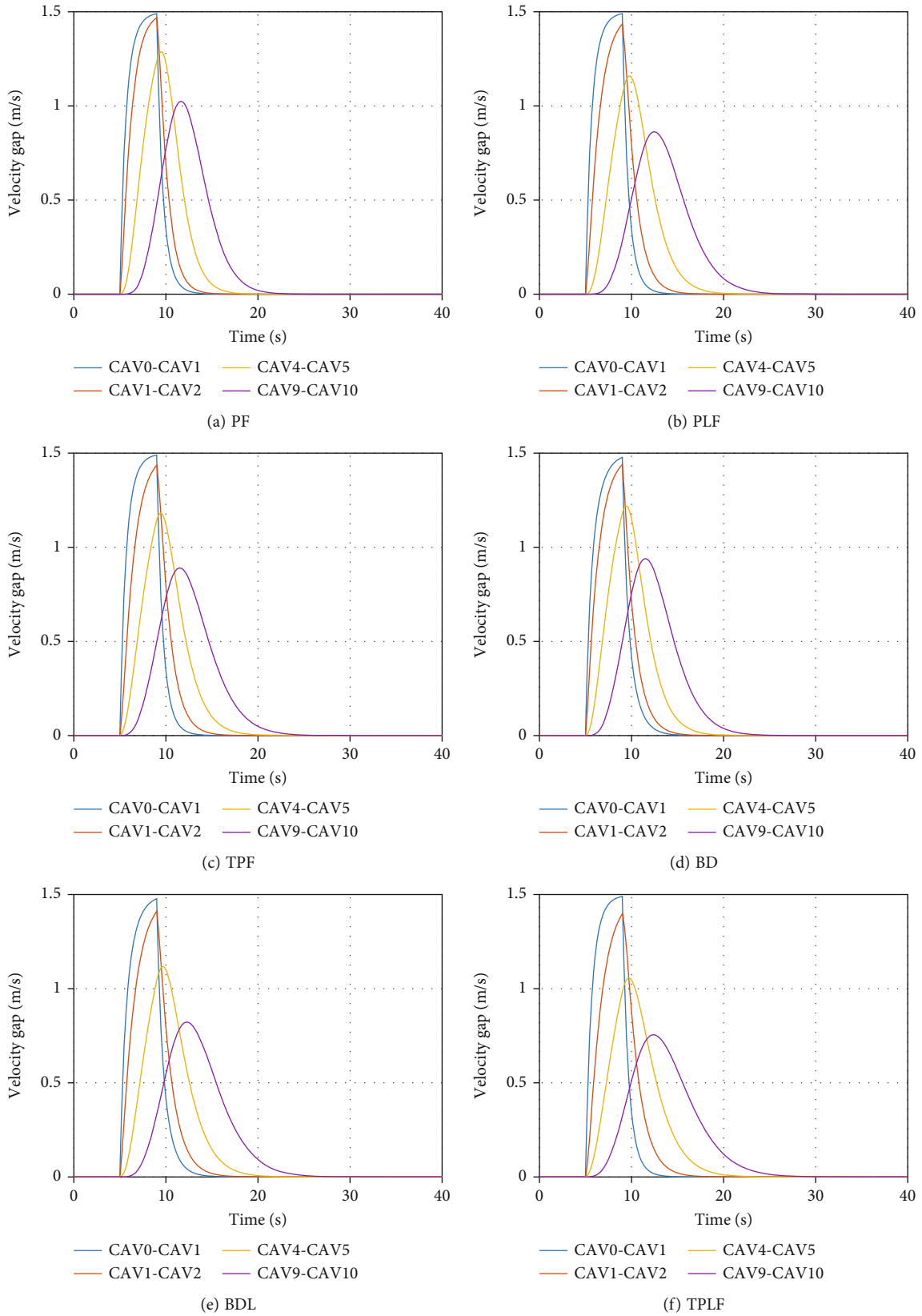

Figure 4: Platoon velocity gap with simulated perturbation under diverse information flow topologies.

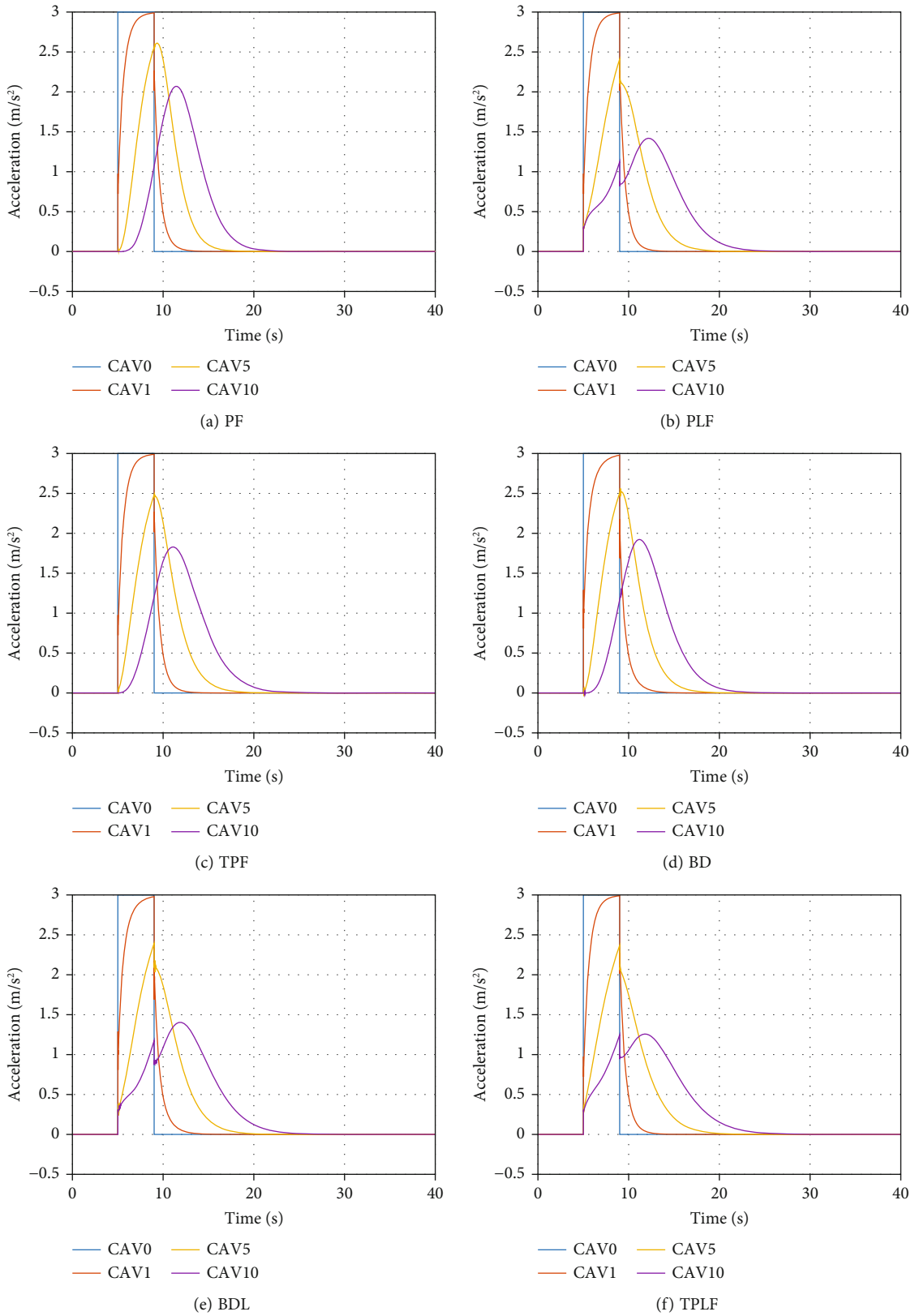

Figure 5: Platoon acceleration with simulated perturbation under diverse information flow topologies.

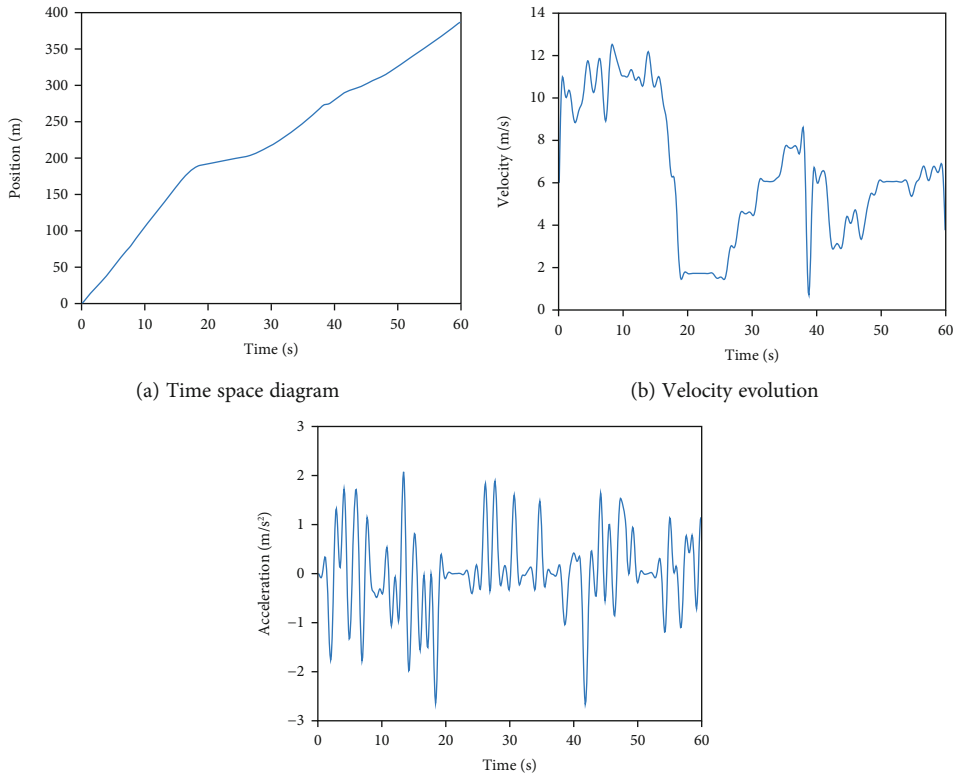

(a) Time space diagram

(b) Velocity evolution

(c) Acceleration evolution

Figure 6: Profiles of vehicle #1992 for I-80 set of NGSIM data.

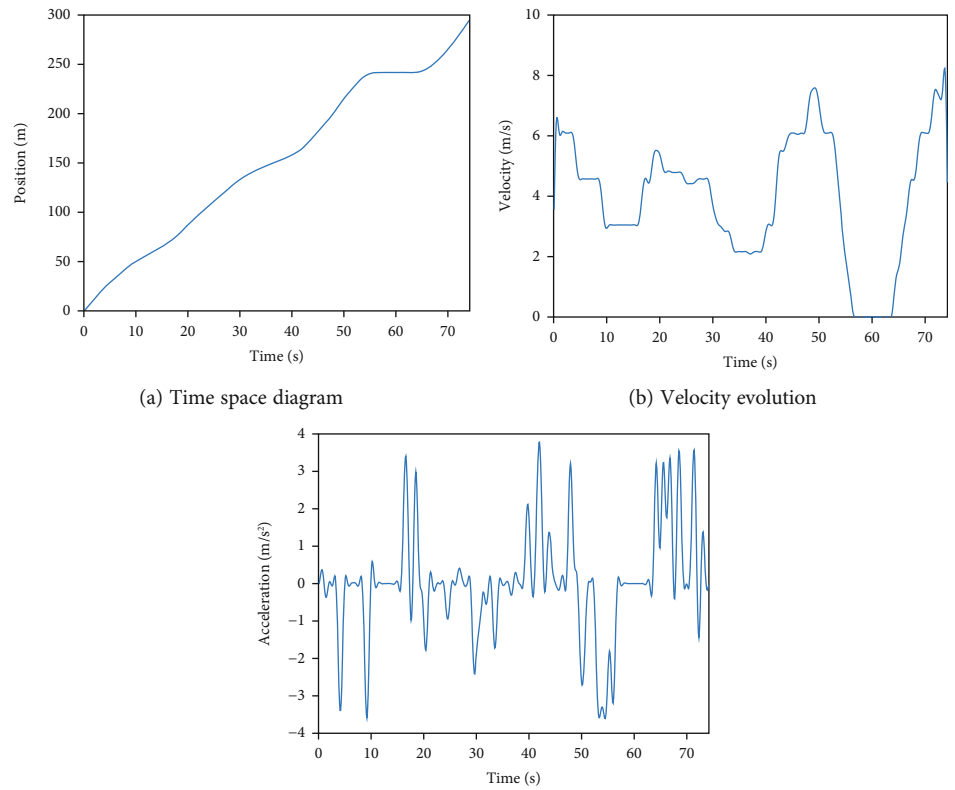

(a) Time space diagram

(b) Velocity evolution

(c) Acceleration evolution

Figure 7: Profiles of vehicle #1635 for US-101 set of NGSIM data.

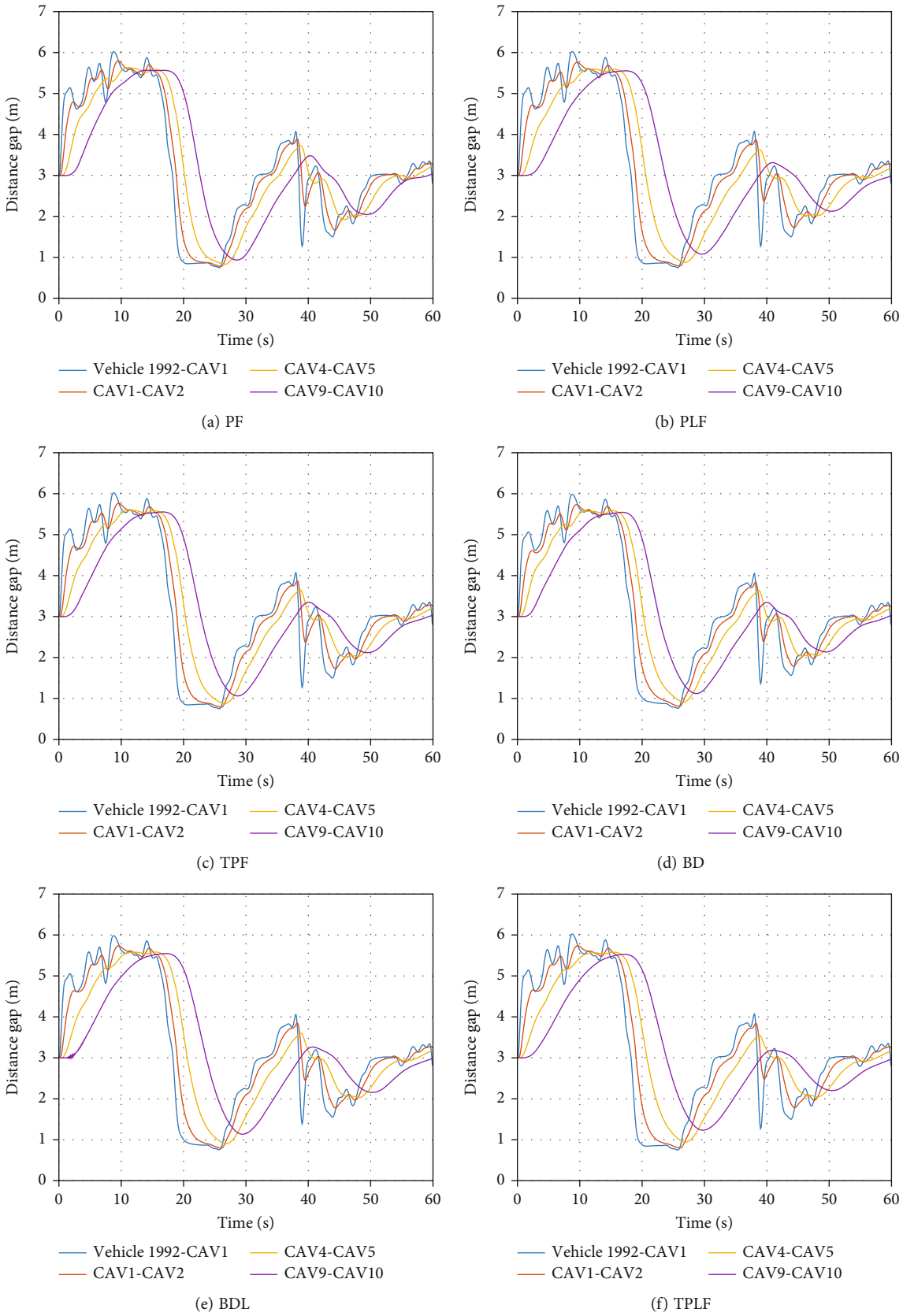

Figure 8: Platoon distance gap with leading vehicle #1992 under diverse information flow topologies.

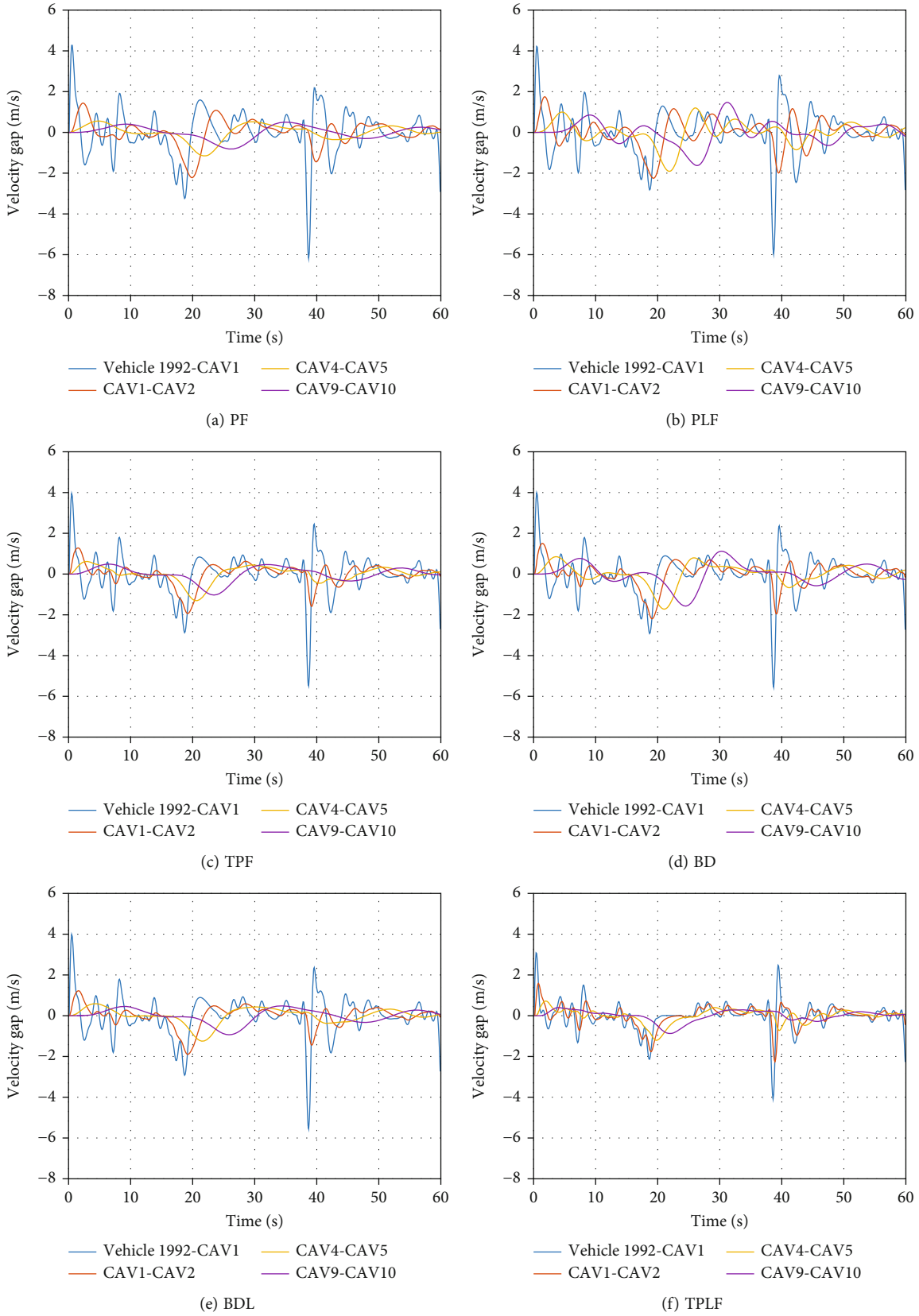

Figure 9: Platoon velocity gap with leading vehicle #1992 under diverse information flow topologies.

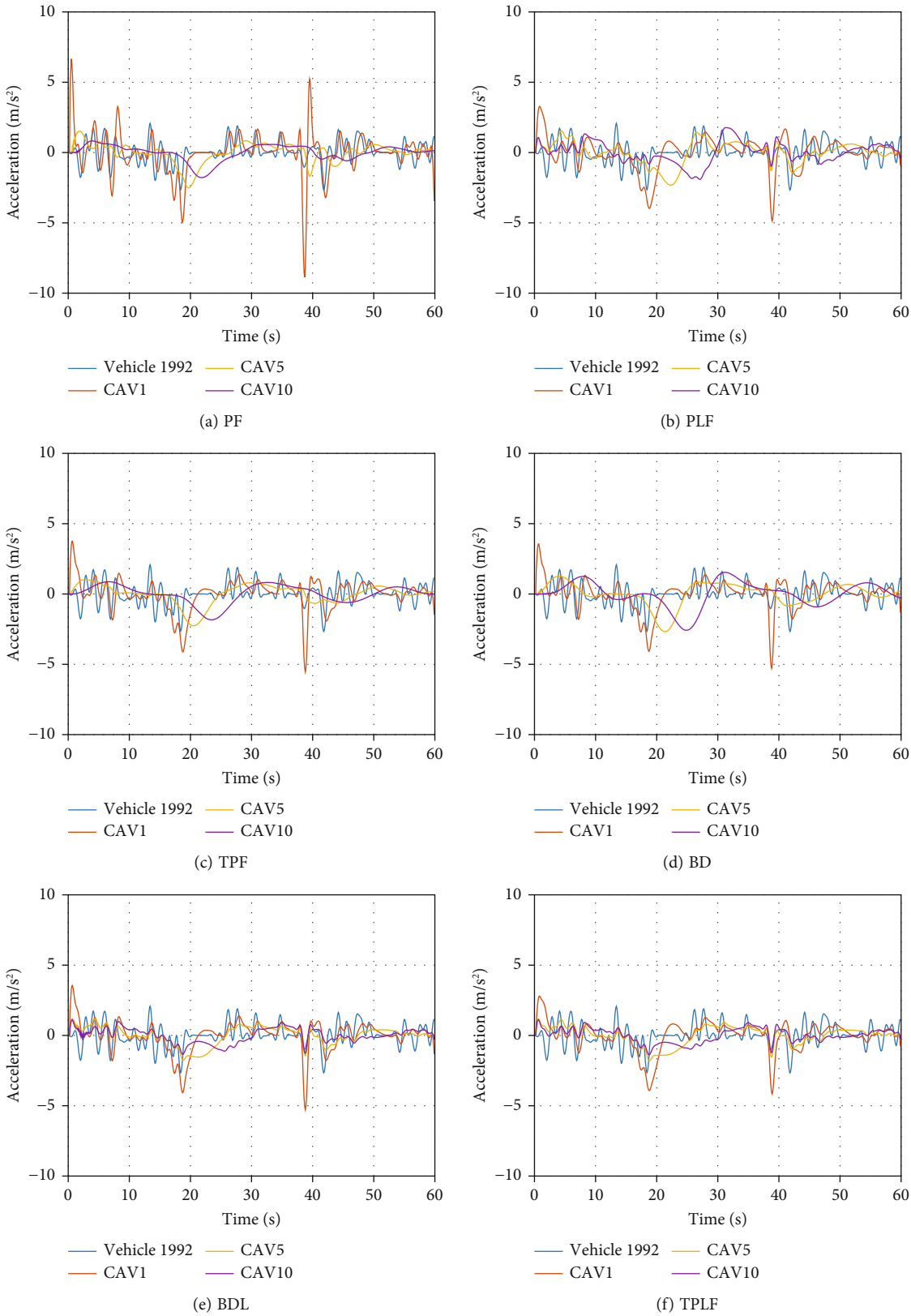

Figure 10: Platoon acceleration with leading vehicle #1992 under diverse information flow topologies.

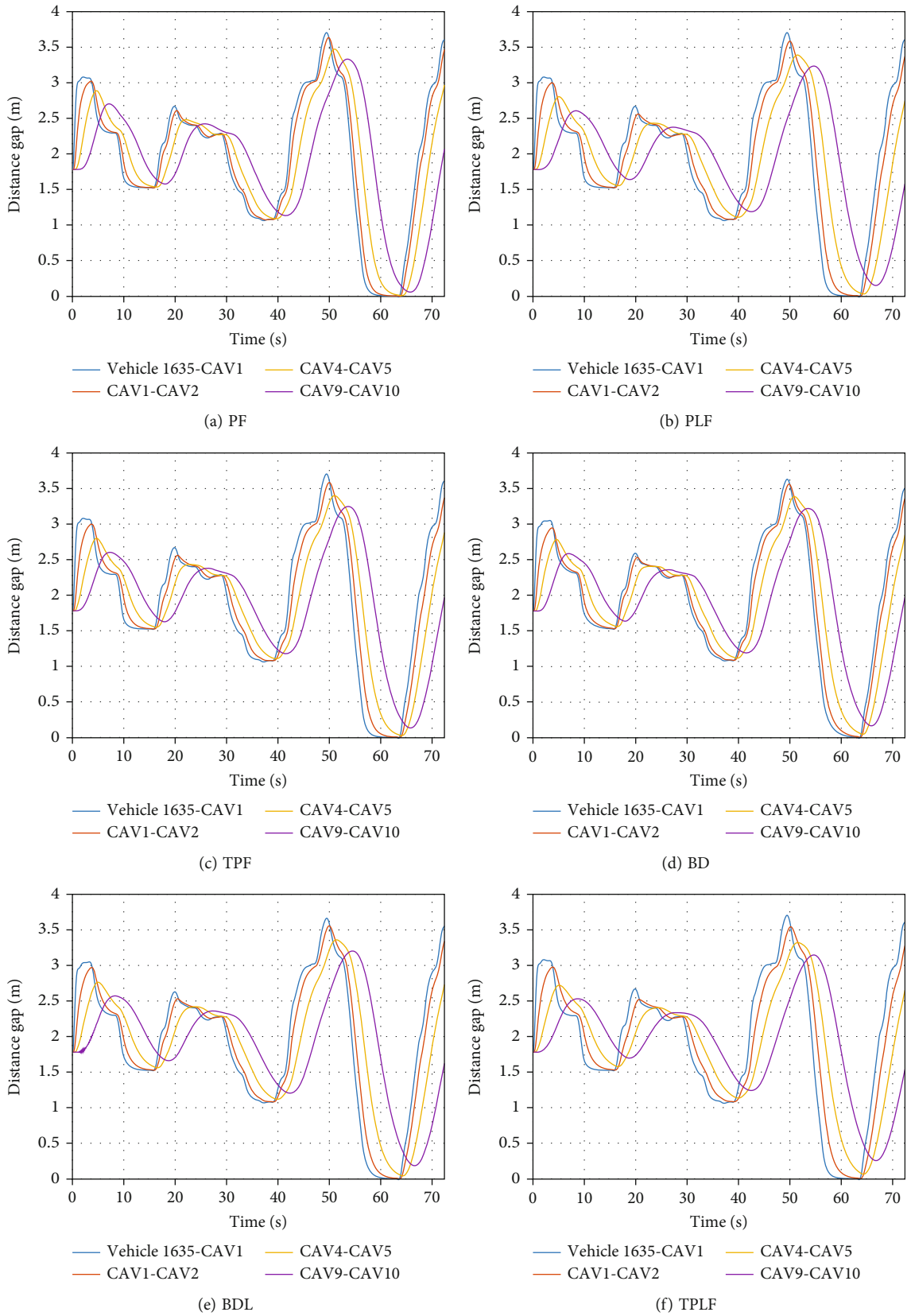

Figure 11: Platoon distance gap with leading vehicle #1635 under diverse information flow topologies.

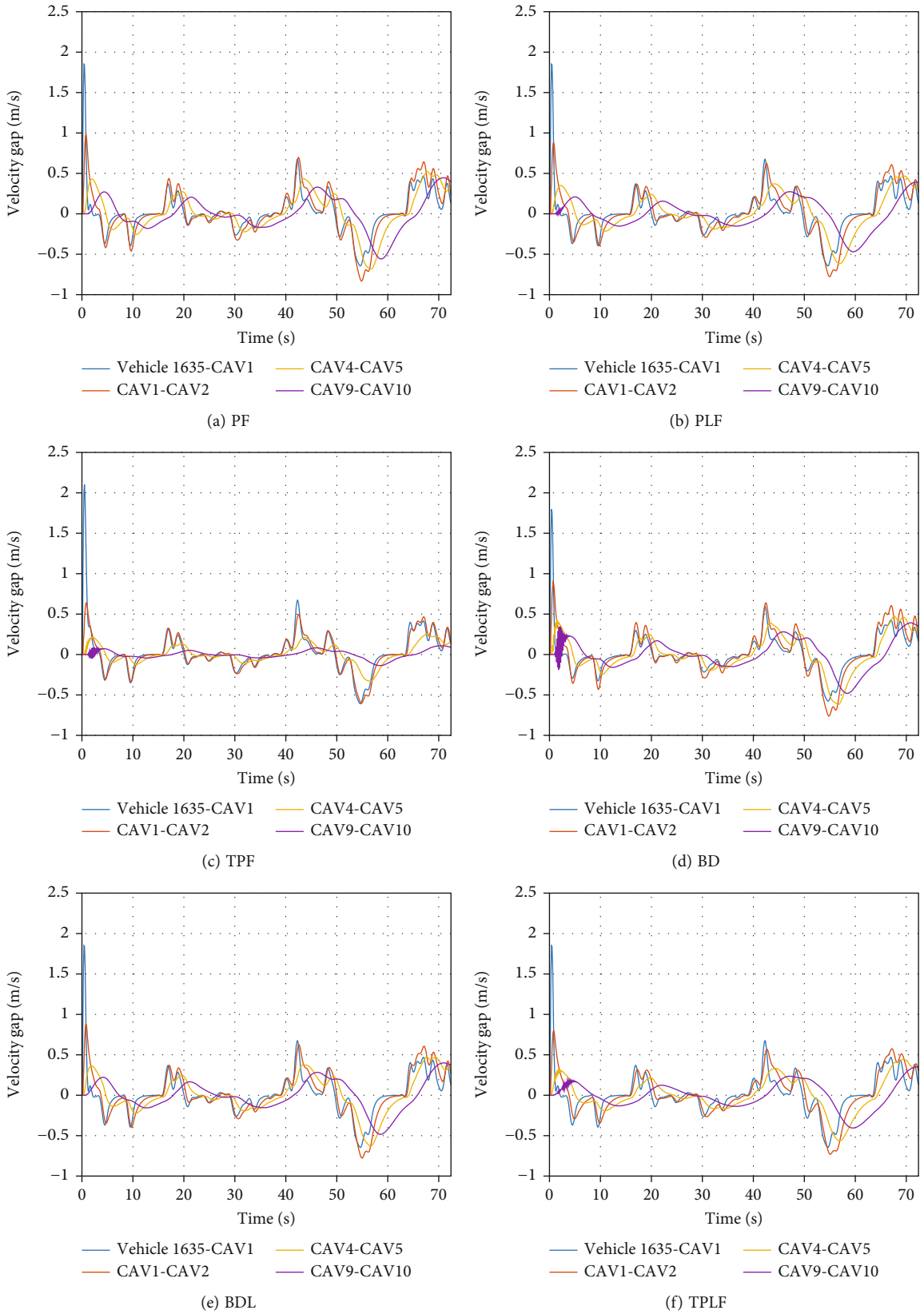

Figure 12: Platoon velocity gap with leading vehicle #1635 under diverse information flow topologies.

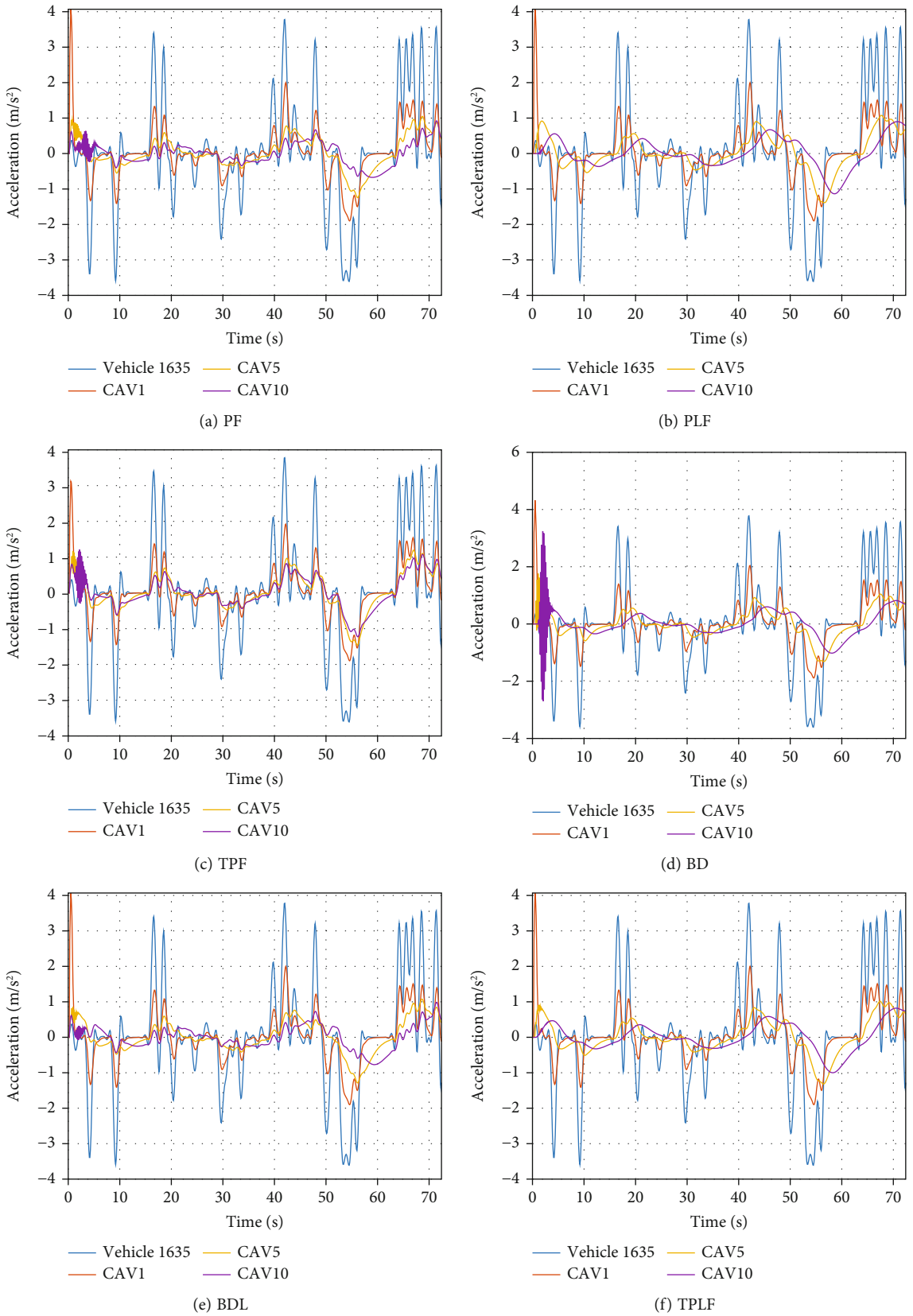

Figure 13: Platoon acceleration with leading vehicle #1635 under diverse information flow topologies.

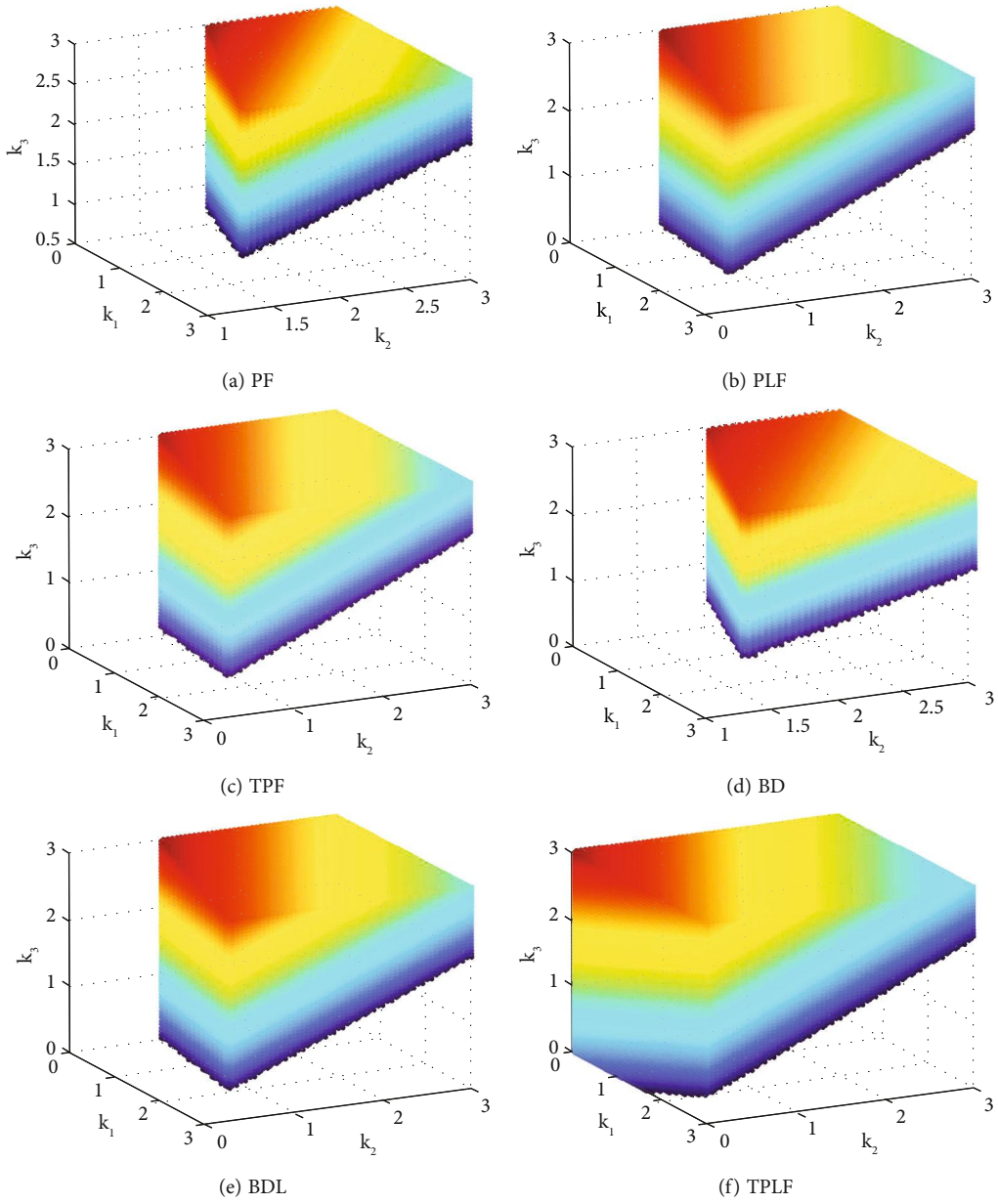

FIGURE 14: Stable region of feedback gains for diverse information flow topologies ($K_L = 1$, $T_L = 0.6$ s).

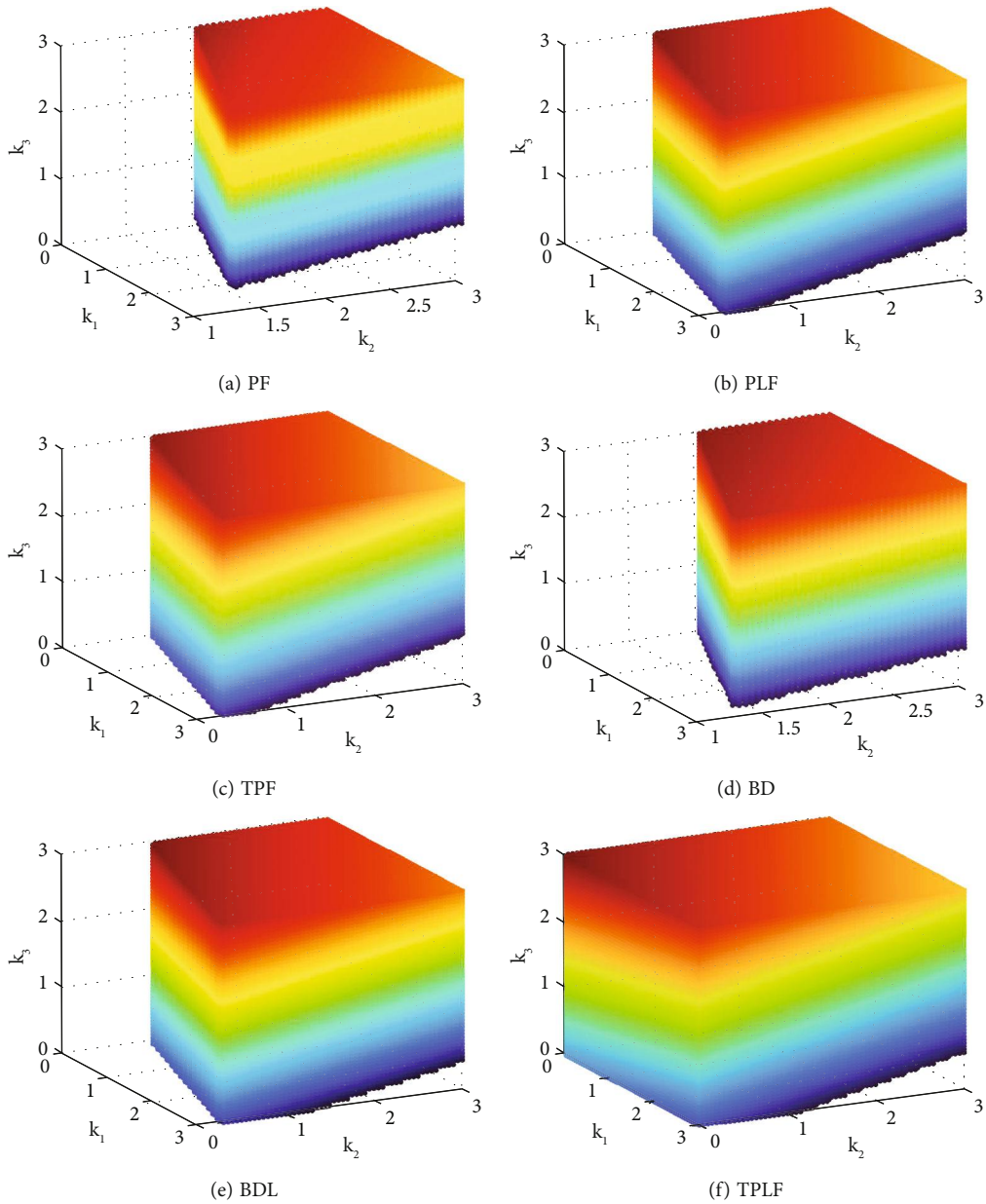

Figure 15: Stable region of feedback gains for diverse information flow topologies ($K_L = 1$, $T_L = 0.3$ s).

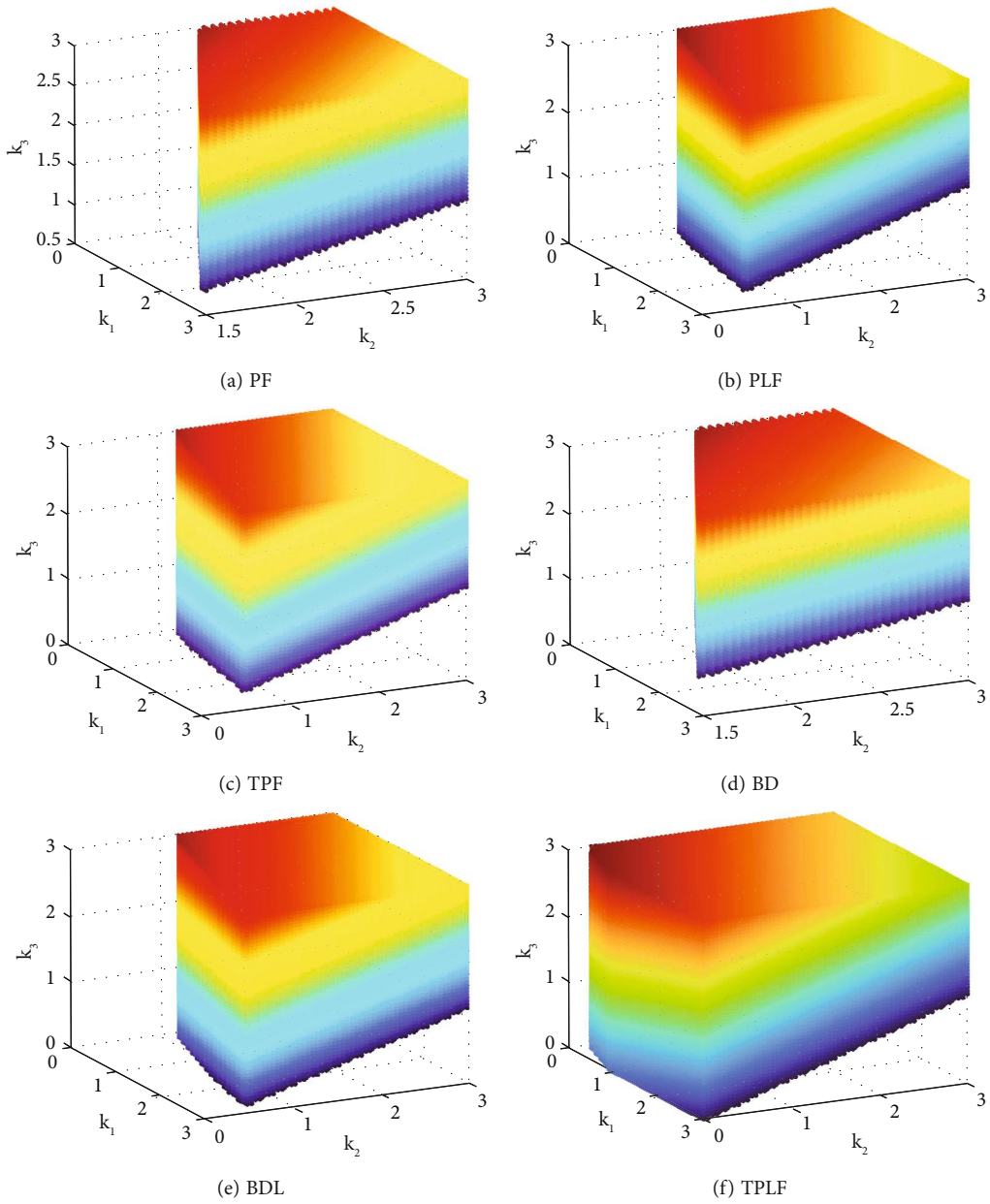

FIGURE 16: Stable region of feedback gains for diverse information flow topologies ($K_L = 0.9$, $T_L = 0.45$ s).

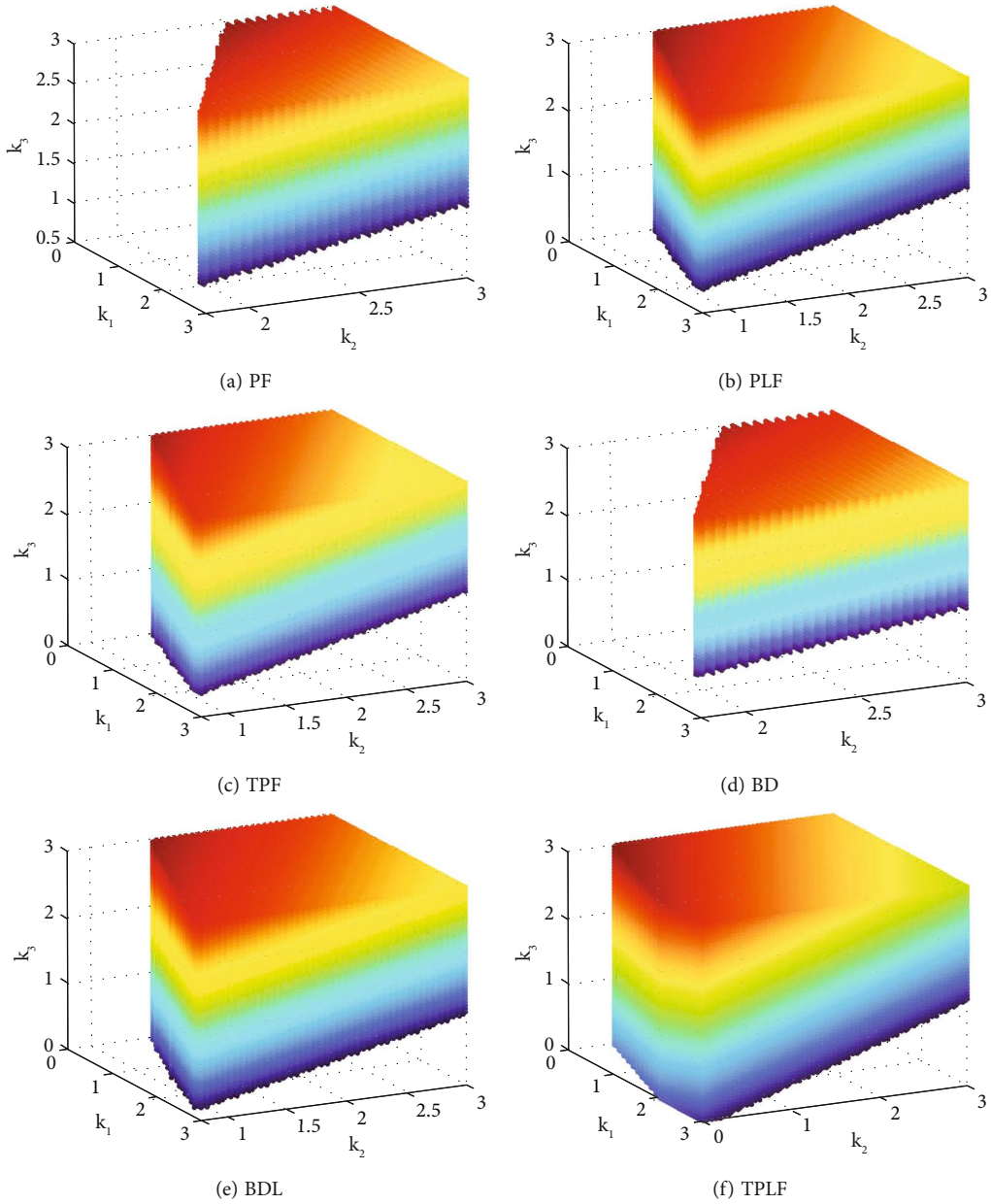

Figure 17: Stable region of feedback gains for diverse information flow topologies ($K_L = 0.8$, $T_L = 0.45$ s).

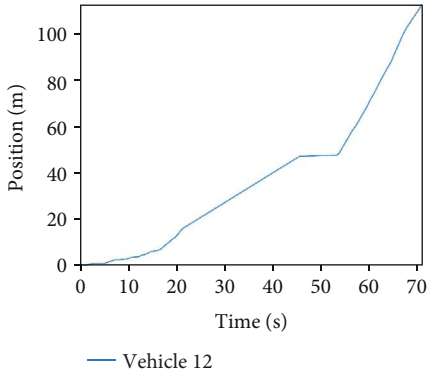

(a) Time space diagram for vehicle 12

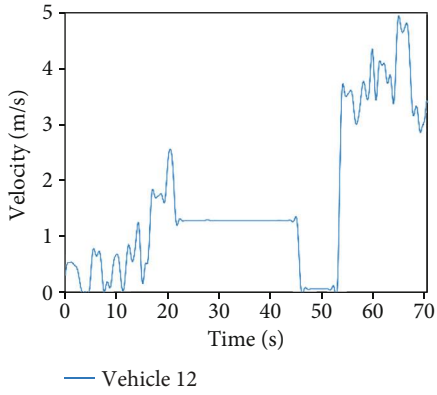

(b) Velocity profiles for vehicle 12

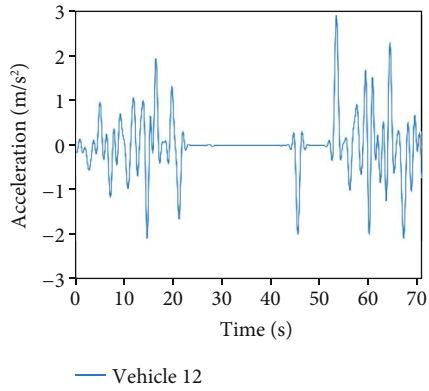

(c) Acceleration profiles for vehicle 12

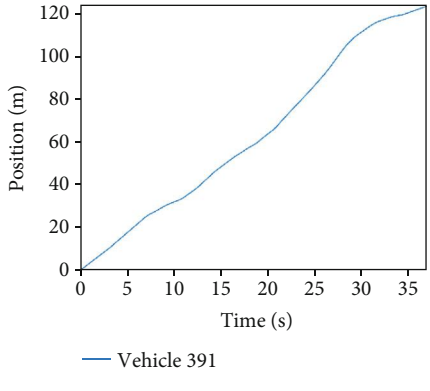

(d) Time space diagram for vehicle 391

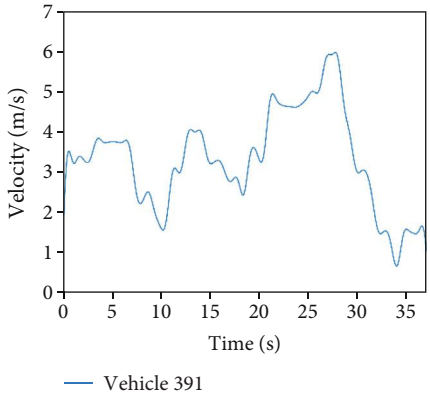

(e) Velocity profiles for vehicle 391

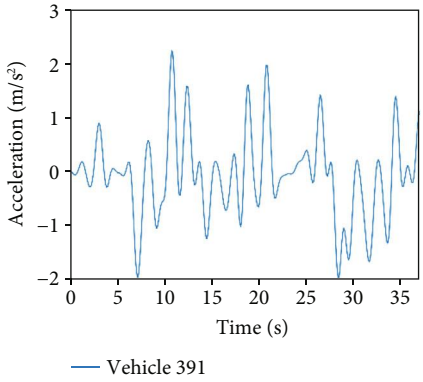

(f) Acceleration profiles for vehicle 391

Figure 18: Continued.

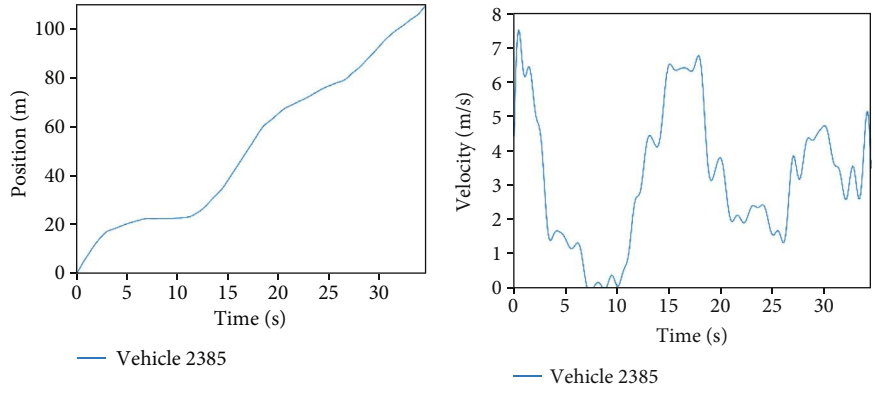

(g) Time space diagram for vehicle 2385

(h) Velocity profiles for vehicle 2385

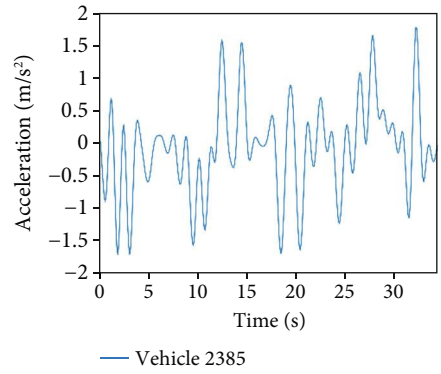

(i) Acceleration profiles for vehicle 2385

Figure 18: Time space diagrams and velocity and acceleration profiles for different vehicles from NGSIM I-80.

Table 2: Safety effects of information flow topologies with different real-world leading vehicles.

	PF	PLF	TPF	BD	BDL	TPLF
Vehicle #1992						
Min TTC	0.28	0.28	0.29	0.29	0.30	0.30
TET	28.4	15.4	18.8	26.9	16.0	11.3
TIT	409.4	326.2	353.8	413.2	339.8	213.9
Vehicle #1635						
Min TTC	0.24	0.27	0.26	0.27	0.27	0.27
TET	3.3	2.2	2.4	2.7	2.3	1.2
TIT	103.1	73.7	84.6	104.5	81.3	57.0
Vehicle #12						
Min TTC	0.27	0.29	0.30	0.30	0.31	0.31
TET	35.6	21.9	23.7	30.8	25.3	19.5
TIT	505.3	354.6	388.4	523.9	372.7	281.0
Vehicle #391						
Min TTC	0.31	0.33	0.32	0.32	0.33	0.33
TET	2.9	2.1	2.2	2.2	2.0	1.4
TIT	81.0	57.2	61.8	85.7	60.3	45.1
Vehicle #2385						
Min TTC	0.26	0.28	0.27	0.28	0.28	0.28
TET	10.2	7.6	7.8	8.0	6.9	4.3
TIT	286.4	211.8	230.2	294.4	226.7	167.5

6. Conclusions

This paper first studies the stability of CACC vehicular platoon under diverse information flow topologies. The CACC longitudinal dynamic model is derived using the exact feedback linearization technique, which accommodates the inertial delay of powertrain dynamics. Accordingly, sufficient conditions of stability are mathematically derived to guarantee distributed frequency-domain-based control parameters. The paper demonstrates that under diverse information flow topologies, with more information a CAV obtains, the larger stable region the platoon system has and the CAV platoon is easier to control for maintaining stability and safety. Further, the information flow topology of TPLF is the most recommended to enhance platoon stability.

Then, this paper assesses the safety of fully CAV platoon under diverse information flow topologies with real-world vehicles as leaders. The safety assessment results demonstrate that the bidirectional type topologies could bring adverse impact on reducing the risk of rear-end collision comparing with other types. Moreover, the predecessor-leader following type topologies contribute to reducing rear-end collision risk. Thus, the information flow topology of TPLF is also recommended to enhance platoon safety.

Unsolved topics for future research include the string stability for heterogeneous platoons under diverse information flow topologies. In addition, there is a need to address CACC vehicular platoon with nonidentical controllers that possess communication delays.

Data Availability

This study is theoretical and does not use personal data. Herein, the simulation involves the open source NGSIM data sets, which can be found in the following website https://ops.fhwa.dot.gov/trafficanalysistools/ngsim.htm.

Conflicts of Interest

The authors declare that they have no known competing financial interests or personal relationships that could have appeared to influence the work reported in this paper.

Authors' Contributions

Yulu Dai is responsible for the conceptualization, methodology, investigation, formal analysis, writing—original draft, and writing—review and editing. Yuwei Yang is assigned to the formal analysis, software, data curation, and visualization. Hongming Zhong, Huijun Zuo, and Qiang Zhang are also involved in the writing—review and editing.

References

[1] J. Guanetti, Y. Kim, and F. Borrelli, "Control of connected and automated vehicles: state of the art and future challenges," *Annual Reviews in Control*, vol. 45, pp. 18–40, 2018.

[2] Y. Li, L. Zhu, H. Wang, F. Yu, and S. Liu, "A cross-layer defense scheme for edge intelligence-enabled CBTC systems against MitM attacks," *IEEE Transactions on Intelligent Transportation Systems*, vol. 22, no. 4, pp. 2286–2298, 2020.

[3] S. E. Shladover, "Connected and automated vehicle systems: introduction and overview," *Journal of Intelligent Transportation Systems*, vol. 22, no. 3, pp. 190–200, 2018.

[4] P. Wang, X. He, Y. Wei, X. Wu, and Y. Wang, "Damping behavior analysis for connected automated vehicles with linear car following control," *Transportation Research Part C: Emerging Technologies*, vol. 138, article 103617, 2022.

[5] Q. Chen, L. Xu, Y. Zhou, and S. Li, "Finite time observer-based super-twisting sliding mode control for vehicle platoons with guaranteed strong string stability," in *IET Intelligent Transport Systems*, John Wiley & Sons, Inc, 2022.

[6] X. Y. Lu and S. Shladover, "Integrated ACC and CACC development for heavy-duty truck partial automation," in *2017 American Control Conference (ACC)*, pp. 4938–4945, Seattle, WA, USA, 2017.

[7] C. Wang, S. Gong, A. Zhou, T. Li, and S. Peeta, "Cooperative adaptive cruise control for connected autonomous vehicles by factoring communication-related constraints," *Transportation Research Part C: Emerging Technologies*, vol. 113, pp. 124–145, 2020.

[8] Q. Chen, Y. Zhou, S. Ahn, J. Xia, S. Li, and S. Li, "Robustly string stable longitudinal control for vehicle platoons under communication failures: a generalized extended state observer-based control approach," *IEEE Transactions on Intelligent Vehicles*, 2022.

[9] M. A. Gordon, F. J. Vargas, A. A. Peters, and A. I. Maass, "Platoon stability conditions under inter-vehicle additive Noisy communication channels," *IFAC-PapersOnLine*, vol. 53, no. 2, pp. 3150–3155, 2020.

[10] J. Wang, Y. H. Kim, X. He, and S. Peeta, "Analytical model for information flow propagation wave under an information relay control strategy in a congested vehicle-to-vehicle communication environment," *Transportation Research Part C: Emerging Technologies*, vol. 94, pp. 1–18, 2018.

[11] Y. Zhou, S. Ahn, M. Chitturi, and D. A. Noyce, "Rolling horizon stochastic optimal control strategy for ACC and CACC under uncertainty," *Transportation Research Part C: Emerging Technologies*, vol. 83, pp. 61–76, 2017.

[12] C. Desjardins and B. Chaib-draa, "Cooperative adaptive cruise control: a reinforcement learning approach," *IEEE Transactions on Intelligent Transportation Systems*, vol. 12, no. 4, pp. 1248–1260, 2011.

[13] S. Öncü, J. Ploeg, N. Van de Wouw, and H. Nijmeijer, "Cooperative adaptive cruise control: network-aware analysis of string stability," *IEEE Transactions on Intelligent Transportation Systems*, vol. 15, no. 4, pp. 1527–1537, 2014.

[14] E. Semsar-Kazerooni, J. Verhaegh, J. Ploeg, and M. Alirezaei, "Cooperative adaptive cruise control: an artificial potential field approach," in *Paper presented at the 2016 IEEE intelligent vehicles symposium (IV)*, pp. 361–367, Gothenburg, Sweden, 2016.

[15] S. E. Shladover, C. Nowakowski, X.-Y. Lu, and R. Ferlis, "Cooperative adaptive cruise control," *Transportation Research Record*, vol. 2489, no. 1, pp. 145–152, 2015.

[16] P. Y. Li and A. Shrivastava, "Traffic flow stability induced by constant time headway policy for adaptive cruise control vehicles," *Transportation Research Part C: Emerging Technologies*, vol. 10, no. 4, pp. 275–301, 2002.

[17] D. Swaroop, J. K. Hedrick, C. C. Chien, and P. Ioannou, "A comparision of spacing and headway control laws for automatically controlled vehicles1," *Vehicle System Dynamics: International Journal of Vehicle Mechanics and Mobility*, vol. 23, no. 1, pp. 597–625, 1994.

[18] Y. Zheng, S. E. Li, J. Wang, D. Cao, and K. Li, "Stability and scalability of homogeneous vehicular platoon: study on the influence of information flow topologies," *IEEE Transactions on Intelligent Transportation Systems*, vol. 17, no. 1, pp. 14–26, 2016.

[19] L. Zhu, Y. Li, F. R. Yu, B. Ning, T. Tang, and X. Wang, "Cross-layer defense methods for jamming-resistant CBTC systems," *IEEE Transactions on Intelligent Transportation Systems*, vol. 22, no. 11, pp. 7266–7278, 2021.

[20] D. Lee, S. Lee, Z. Chen, B. B. Park, and D. H. Shim, "Design and field evaluation of cooperative adaptive cruise control with unconnected vehicle in the loop," *Transportation Research Part C: Emerging Technologies*, vol. 132, article 103364, 2021.

[21] D. Ngoduy, "Linear stability of a generalized multi-anticipative car following model with time delays," *Communications in Nonlinear Science and Numerical Simulation*, vol. 22, no. 1, pp. 420–426, 2015.

[22] Z. Wu, J. Sun, and R. Xu, "Consensus-based connected vehicles platoon control via impulsive control method," *Physica A: Statistical Mechanics and its Applications*, vol. 580, article 126190, 2021.

[23] L. Zhu, H. Liang, H. Wang, B. Ning, and T. Tang, "Joint security and train control design in blockchain-e mpowered CBTC system," *IEEE Internet of Things Journal*, vol. 9, no. 11, pp. 8119–8129, 2022.

[24] D. Swaroop and J. K. Hedrick, "Constant spacing strategies for platooning in automated highway systems," *Journal of Dynamic Systems, Measurement, and Control*, vol. 121, no. 3, pp. 462–470, 1999.

[25] P. Seiler, A. Pant, and K. Hedrick, "Disturbance propagation in vehicle strings," *IEEE Transactions on Automatic Control*, vol. 49, no. 10, pp. 1835–1841, 2004.

[26] A. Ghasemi, R. Kazemi, and S. Azadi, "Stability analysis of bidirectional adaptive cruise control with asymmetric information flow," *Proceedings of the Institution of Mechanical Engineers, Part C: Journal of Mechanical Engineering Science*, vol. 229, no. 2, pp. 216–226, 2015.

[27] Y. Hu, T. Ma, and J. Chen, "Multi-anticipative bi-directional visual field traffic flow models in the connected vehicle environment," *Physica a: Statistical Mechanics and its Applications*, vol. 584, article 126372, 2021.

[28] J. Ploeg, N. Van De Wouw, and H. Nijmeijer, "Lp string stability of cascaded systems: application to vehicle platooning," *IEEE Transactions on Control Systems Technology*, vol. 22, no. 2, pp. 786–793, 2014.

[29] M. Treiber and A. Kesting, *Traffic Flow Dynamics*, Springer-Verlag, Berlin Heidelberg, 2013.

[30] R. E. Wilson and J. A. Ward, "Car-following models: fifty years of linear stability analysis - a mathematical perspective," *Transportation Planning and Technology*, vol. 34, no. 1, pp. 3–18, 2011.

[31] Y. Zhou, S. Ahn, M. Wang, and S. Hoogendoorn, "Stabilizing mixed vehicular platoons with connected automated vehicles: an H-infinity approach," *Transportation Research Procedia*, vol. 38, pp. 441–461, 2019.

[32] K. Yi and Y. D. Kwon, "Vehicle-to-vehicle distance and speed control using an electronic-vacuum booster," *JSAE Review*, vol. 22, no. 4, pp. 403–412, 2001.

[33] D. Swaroop and J. K. Hedrick, "String stability of interconnected systems," *IEEE Transactions on Automatic Control*, vol. 41, no. 3, pp. 349–357, 1996.

[34] K. Li, C. Zou, S. Bu, Y. Liang, J. Zhang, and M. Gong, "Multi-modal feature fusion for geographic image annotation," *Pattern Recognition*, vol. 73, pp. 1–14, 2018.

[35] P. C. Parks, "A new proof of the Routh-Hurwitz stability criterion using the second method of Liapunov," *Mathematical Proceedings of the Cambridge Philosophical Society*, vol. 58, no. 4, pp. 694–702, 1962.

[36] G. J. Naus, R. P. Vugts, J. Ploeg, M. J. van De Molengraft, and M. Steinbuch, "String-stable CACC design and experimental validation: a frequency-domain approach," *IEEE Transactions on Vehicular Technology*, vol. 59, no. 9, pp. 4268–4279, 2010.

[37] Y. Zhou and S. Ahn, "Robust local and string stability for a decentralized car following control strategy for connected automated vehicles," *Transportation Research Part B: Methodological*, vol. 125, pp. 175–196, 2019.

[38] M. Montanino and V. Punzo, "Trajectory data reconstruction and simulation-based validation against macroscopic traffic patterns," *Transportation Research Part B: Methodological*, vol. 80, pp. 82–106, 2015.

[39] V. Punzo, M. T. Borzacchiello, and B. Ciuffo, "On the assessment of vehicle trajectory data accuracy and application to the Next Generation SIMulation (NGSIM) program data," *Transportation Research Part C: Emerging Technologies*, vol. 19, no. 6, pp. 1243–1262, 2011.

[40] M. S. Rahman and M. Abdel-Aty, "Longitudinal safety evaluation of connected vehicles' platooning on expressways," *Accident Analysis and Prevention*, vol. 117, pp. 381–391, 2018.

[41] Y. Li, Z. Li, H. Wang, W. Wang, and L. Xing, "Evaluating the safety impact of adaptive cruise control in traffic oscillations on freeways," *Accident Analysis & Prevention*, vol. 104, pp. 137–145, 2017.